

Ultraviolet flux and spectral variability study of blazars observed with UVIT/*AstroSat*

M. RESHMA,¹ ADITI AGARWAL,² C. S. STALIN,³ PRAJWEL JOSEPH,^{3,1} AKANKSHA DAGORE,³ AMIT KUMAR MANDAL,⁴ ASHISH DEVARAJ,¹ AND S. B. GUDENNAVAR¹

¹Department of Physics and Electronics, CHRIST University, Bangalore 560 029, India

²Centre for Cosmology and Science Popularization, SGT University, Gurugram 122 505, India

³Indian Institute of Astrophysics, Block II, Koramangala, Bangalore 560 034, India

⁴Department of Physics & Astronomy, Seoul National University, Seoul 08826, Republic of Korea

ABSTRACT

Blazars, the peculiar class of active galactic nuclei (AGN), are known to show flux variations across the accessible electromagnetic spectrum. Though they have been studied extensively for their flux variability characteristics across wavelengths, information on their ultraviolet (UV) flux variations on time scales of hours is very limited. Here, we present the first UV flux variability study on intraday time scales of a sample of 10 blazars comprising 2 flat spectrum radio quasars (FSRQs) and 8 BL Lacertae objects (BL Lacs). These objects, spanning a redshift (z) range of $0.034 \leq z \leq 1.003$, were observed in the far-UV (FUV: 1300 – 1800 Å) and near-UV (NUV: 2000 – 3000 Å) wavebands using the ultraviolet imaging telescope on board *AstroSat*. UV flux variations on time scales of hours were detected in 9 sources out of the observed 10 blazars. The spectral variability analysis showed a bluer-when-brighter trend with no difference in the UV spectral variability behavior between the studied sample of FSRQs and BL Lacs. The observed UV flux and spectral variability in our sample of both FSRQs and BL Lacs revealed that the observed UV emission in them is dominated by jet synchrotron process.

Keywords: Active galactic nuclei (16) - Blazars (164) - BL Lac objects (168) - flat spectrum radio quasars (2163) - Ultraviolet photometry (1740)

1. INTRODUCTION

Active Galactic Nuclei (AGN), the high luminosity ($10^{11} - 10^{14} L_{\odot}$) sources in the Universe, are thought to be powered by the accretion of matter onto super massive black holes (SMBHs: $10^6 - 10^{10} M_{\odot}$) situated at the center of galaxies (Lynden-Bell 1969; Rees 1984). About 10% of AGN emit copiously in the radio band, display relativistic jets, and emit over a wide range of the electromagnetic spectrum from low energy radio waves to high energy (TeV) γ -rays. A minority of these objects having their relativistic jets oriented close to the line of sight to the observer ($\leq 10^\circ$) are called blazars (Antonucci 1993; Urry & Padovani 1995). The broad band spectral energy distribution (SED) of blazars is dominated by the beamed emission from relativistic particles in their jet (Blandford & Rees 1978; Urry & Padovani

1995).

Blazars are divided into flat spectrum radio quasars (FSRQs) and BL Lacertae objects (BL Lacs), with FSRQs having broad emission lines with equivalent width above 5 Å and BL Lacs having either a featureless spectra or spectra with weak emission lines with equivalent width below 5 Å. A more physical distinction between FSRQs and BL Lacs is based on the luminosity of the broad line region (L_{BLR}) relative to the Eddington luminosity (L_{Edd}) with the dividing line set at $L_{BLR}/L_{Edd} \sim 5 \times 10^{-4}$ (Ghisellini et al. 2011). The broad band SED of blazars has a two hump structure. The low energy hump peaking in the optical/infrared/soft X-ray region is attributed to synchrotron emission process (Urry & Mushotzky 1982) and the high energy hump peaking in the X-ray/MeV region is attributed to inverse Compton scattering process (Abdo et al. 2010). Based on the position of the synchrotron peak (ν_{peak}) in their broad band SED, blazars are further divided into low synchrotron peaked (LSP; $\nu_{peak} < 10^{14}$ Hz), intermedi-

Corresponding author: C. S. Stalin; S. B. Gudennavar
 stalin@iiap.res.in; shivappa.b.gudennavar@christuniversity.in

ate synchrotron peaked (ISP; 10^{14} Hz $<$ ν_{peak} $<$ 10^{15} Hz) and high synchrotron peaked (HSP; $\nu_{peak} > 10^{15}$ Hz) blazars (Abdo et al. 2010).

In addition, an important characteristic of blazars is that they show flux variations over the entire accessible electromagnetic spectrum on a range of time scales from minutes to hours (Wagner & Witzel 1995; Ulrich et al. 1997; Webb 2021). Such flux variations can serve as an efficient tool to understand the nature of the central regions and the jets of blazars. The flux variations are also known to be correlated across wavelengths, supporting the argument that the low energy and the high energy emission arises from the same population of relativistic electrons in the jet via synchrotron and inverse Compton processes, respectively (Ulrich et al. 1997). However, recent observations point to varied correlations between low energy optical and high energy γ -ray observations indicating lack of our understanding on the flux variability characteristics of blazars (Rajput et al. 2020, 2021). In addition to flux variations, blazars also show large optical and infrared polarization (Angel & Stockman 1980) and optical polarization variations (Rakshit et al. 2017; Pandey et al. 2022; Rajput et al. 2022). Though blazars have been studied for variability across multiple wavelengths, on a range of time scales, their ultraviolet (UV) variability characteristics are not explored much, with only sparse reports available in the literature (Edelson 1992). Understanding the UV flux variations in blazars is important as the UV emission in the broad band SED of blazars is usually dominated by synchrotron emission from relativistic jet electrons (Abdo et al. 2011; Paliya et al. 2015). However, in the faint state, signature of prominent accretion disk emission in the optical-UV region is evident in the broad band SED of the FSRQ category of blazars (Bonnoli et al. 2011; Paliya et al. 2016, 2017). Some recent studies do exist that focus on UV variability of AGN sources, mainly from *Galaxy Evolution Explorer (GALEX)* and *International Ultraviolet Explorer (IUE)* observations (Welsh et al. 2011; Sukanya et al. 2018). However, these studies are focused on flux variations in non-blazar type AGN on longer time scales.

In this work, UV variability characteristics of blazars on hour-like time scales are studied using the data from the ultraviolet imaging telescope (UVIT: Tandon et al. 2017, 2020) on board *AstroSat*. This is the first study where the temporal and spectral properties of 10 blazars in UV on intraday time scales are investigated. The paper is structured as follows: In Section 2, observations and data reduction procedures are described. In Section 3, the analysis technique used to study the temporal and spectral variability properties of the sample of sources is

Table 1. Details of the sources studied in this work. Here, RA, Dec., and z are the right ascension, declination, and redshift of the sources, respectively (Veron-Cetty & Veron 2010). FS refers to FSRQ and BL refers to BL Lac, LSP and HSP refer to low synchrotron peaked and high synchrotron peaked blazars.

Name	RA (hh:mm:ss)	Dec. (dd:mm:ss)	Type / Subtype	z
PKS 0208–512	02:10:46.20	−51:01:01.89	FS/LSP	1.003
1ES 0229+200	02:32:48.62	+20:17:17.48	BL/HSP	0.140
OJ 287	08:54:48.88	+20:06:30.64	BL/LSP	0.306
1ES 1101–232	11:03:37.61	−23:29:31.20	BL/HSP	0.186
1ES 1218+304	12:21:21.94	+30:10:37.16	BL/HSP	0.182
H 1426+428	14:28:32.61	+42:40:21.05	BL/HSP	0.129
PKS 1510–089	15:12:50.53	−09:05:59.83	FS/LSP	0.360
Mrk 501	16:53:52.22	+39:45:36.61	BL/HSP	0.034
PKS 2155–304	21:58:52.07	−30:13:32.12	BL/HSP	0.116
1ES 2344+514	23:47:04.84	+51:42:17.88	BL/HSP	0.044

detailed, while the notes on individual sources and the results are detailed in Section 4. Finally, discussion and conclusions are presented in Section 5.

2. OBSERVATIONS AND DATA REDUCTION

The sample of sources used for this study was selected from the archives of observations carried out by UVIT (Tandon et al. 2017, 2020), one of the payloads on board India’s multi-wavelength astronomical observatory, *AstroSat* (Agrawal 2017), launched by the Indian Space Research Organization on 28 September 2015. UVIT with a field of view of ~ 28 arcmin diameter observes simultaneously in two channels namely, the far-UV (FUV: 1300 – 1800 Å) and the near-UV (NUV: 2000 – 3000 Å) using a set of filters. It also has a visual (VIS) channel (3200 – 5500 Å), which is used for tracking the aspects of the telescope, and is used in the processing of the data while generating science-ready images in the FUV and NUV channels. The details of the sources studied in this work are given in Table 1. The log of observations of the sources used in this work is given in Table 2 and the details of the filters used are given in Table 3. The science-ready images of the observations available at the Indian Space Science Data Center (ISSDC)¹ are used in this work. The images were made available to ISSDC by the Payload Operations Center (POC) at the Indian Institute of Astrophysics, Bangalore. At the POC, the

¹ <https://www.issdc.gov.in/astro.html>

Table 2. Log of observations. Here, name of the source, date of observation (dd-mm-yyyy), observational ID (OBSID), filters used in the observations, start and end time of the observations in modified julian date (MJD) and the net exposure time in seconds are given in columns 1, 2, 3, 4, 5, 6 and 7, respectively.

Name	Date of observation	OBSID	Filter	MJD Start	MJD End	Net exposure time
PKS 0208–512	30-10-2016	A02-114T01-9000000764	F148W	57690.991247	57691.386868	1337
			F169M	57691.588337	57691.731484	1710
			N219M	57690.991175	57691.524076	2236
			N279N	57691.588288	57691.863146	2119
	25-12-2019	T03-170T01-9000003388	F148W	58841.831743	58841.833213	119
			F154W	58841.904312	58841.905736	116
			F169M	58841.976881	58842.311886	1223
			F172M	58842.508345	58842.654596	1037
			F154W	58027.768812	58027.926301	4922
			N245M	58027.768763	58027.926351	4951
1ES 0229+200	01-10-2017	A04-130T01-9000001572	F154W	58096.737591	58096.944207	4970
			N245M	58096.737542	58096.944257	5005
	09-12-2017	A04-130T01-9000001762	F154W	58108.834869	58109.180995	3962
			N245M	58108.834820	58109.109934	5046
			F154W	58126.562901	58126.779650	4974
OJ 287	22-12-2017	A04-130T01-9000001792	N245M	58126.562852	58126.779700	5006
			F154W	58126.562901	58126.779650	4974
			N245M	58126.779650	58126.779700	5006
	08-01-2018	A04-130T01-9000001822	F154W	57852.921707	57853.686358	8422
			N245M	57852.921656	57853.415465	4501
			N263M	57853.417144	57853.686437	3649
	18-04-2018	A04-199T01-9000002040	F169M	58225.694593	58227.596754	25365
			F172M	58223.458444	58225.692828	28154
			F148W	58984.390970	58984.732999	3636
1ES 1101–232	18-05-2020	T03-206T01-9000003672	F154W	58984.734732	58985.407435	4855
			F172M	58986.764797	58987.710244	6497
			F148Wa	58985.409168	58986.561064	3782
	30-12-2016	G06-086T02-9000000936	F154W	57750.400520	57752.501664	33497
			N263M	57750.400471	57752.501714	33926
			F148W	57528.302435	57529.431526	13881
1ES 1218+304	21-05-2016	G05-211T01-9000000464	N245M	57528.302745	57529.431577	13847
			F148W	58181.865544	58182.463086	6836
	05-03-2018	A04-094T01-9000001942	F154W	58181.577434	58181.863807	7940
			N242W	58181.577385	58181.781955	5110
H 1426+428	15-06-2018	A04-101T01-9000002170	N245M	58181.783577	58182.463086	9772
			F148W	57476.398455	57478.031161	26663
			N219M	57476.398407	57478.031211	26866
			F172M	58192.878269	58193.695960	13270
	15-06-2018	A04-101T01-9000002170	N219M	58192.878220	58193.696009	13349
			F172M	58284.086589	58284.771371	12085
			F154W	57615.260263	57615.946790	12154
Mrk 501	15-08-2016	G05-218T05-9000000602	N219M	57615.255611	57615.946840	12639
			F148W	58935.087363	58937.726873	25484
	28-03-2020	A07-145T01-9000003594	F154W	58259.329918	58259.544023	2788
			F154W	58293.495067	58293.579373	2842
			F154W	58742.571362	58742.777812	4117
PKS 2155–304	16-09-2019	A05-117T01-9000003166	F154W	57910.717527	57910.863068	2195
			N245M	57910.717477	57910.860639	2015
			F172M	57943.391924	57943.546931	3586
	09-07-2017	A03-033T01-9000001368	N245M	57943.391873	57943.549083	3718
			F172M	57972.282651	57972.430529	3886
			N245M	57972.282601	57972.428121	3705
	07-08-2017	A03-033T01-9000001438	F172M	58003.815110	58003.972611	3977
			N245M	58003.815060	58003.972663	4000
			F172M	58078.933083	58079.201251	1897
1ES 2344+514	07-12-2017	A04-049T01-9000001710	N245M	58094.972718	58095.243561	1392
			F172M	58094.972670	58095.243611	1409
	12-09-2018	T02-104T01-9000002356	N245M	58094.972670	58095.243611	1409
			F172M	58372.864037	58373.064969	3439

Table 3. Details of FUV and NUV filters of UVIT used in this work. Here, λ_{mean} is the mean wavelength and $\Delta\lambda$ is the bandwidth (Tandon et al. 2020).

Filter	λ_{mean} (Å)	$\Delta\lambda$ (Å)	Zero point (mag)
F148W	1481	500	18.097 ± 0.010
F148Wa	1485	500	18.097 ± 0.010
F154W	1541	380	17.771 ± 0.010
F169M	1608	290	17.410 ± 0.010
F172M	1717	125	16.274 ± 0.020
N242W	2418	785	19.763 ± 0.002
N219M	2196	270	16.654 ± 0.020
N245M	2447	280	18.452 ± 0.005
N263M	2632	275	18.146 ± 0.010
N279N	2792	90	16.416 ± 0.010

images were reduced using the UVIT L2 pipeline version 6.3 (Ghosh et al. 2021, 2022). The pipeline creates science-ready images by correcting the raw data for spacecraft drift, flat field, and geometric distortion. The observed fields of the sources are given in Fig. 1. The aperture photometry for one of the target sources, 1ES 1218+304, for a radius of 12 sub-pixels was carried out using the *Photutils* Python package (Bradley et al. 2023). Background was removed using the local background subtraction method, where a circular annular region with an inner radius of 150 sub-pixels and an outer radius of 200 sub-pixels were used. The background-subtracted source light curve obtained using *Photutils* was compared with the light curve generated using the *Curvit* Python package (Joseph et al. 2021) (Fig. 2). From Fig. 2, it is evident that both the light curves are very well matched. The mean of the difference light curve (bottom panel of Fig. 2) was found to be 0.016 ± 0.003 mag. This is due to the systematically fainter magnitudes from *Photutils* as the derived magnitudes were not corrected for saturation effects. The advantage of *Curvit* over *Photutils* is that *Curvit* works on the calibrated events list, while *Photutils* works on the images. Therefore, for the rest of the sample sources, the *Curvit* package (Joseph et al. 2021) was used to generate the light curves. In each source, the individual orbit-wise events list were combined using *Curvit* package and the combined events list was used for generating the light curves. In addition to background subtraction, the light curves were also subjected to aperture and saturation correction. The brightness of the blazars derived over a circular aperture of 12 sub-pixel radii using *Curvit* was then converted to the total brightness using Table 11 of

Tandon et al. (2020). The brightness of all the blazars thus obtained is given in the Appendix.

3. ANALYSIS

3.1. Flux variability

The intrinsic amplitude of flux variability, which is basically the observed variance of the light curve after the removal of the measurement errors, was calculated to characterize variability. The intrinsic amplitude of flux variability, σ_m (mag), is defined as (Ai et al. 2010),

$$\sigma_m = \sqrt{(\Sigma^2 - \epsilon^2)} \quad (1)$$

Here, Σ^2 is the observed variance and is given by

$$\Sigma = \sqrt{\frac{1}{N-1} \sum_{i=1}^N (m_i - \langle m \rangle)^2} \quad (2)$$

where, N is the number of orbits, $\langle m \rangle$ is the weighted mean of the m_i measurements with errors ϵ_i . ϵ is the contribution of measurement errors to the variance and is defined as

$$\epsilon^2 = \frac{1}{N} \sum_{i=1}^N \epsilon_i^2 \quad (3)$$

A source was considered variable if $\Sigma^2 > \epsilon^2$, else, $\sigma_m = 0$.

3.2. Spectral variability

In order to study the various spectral trends found in blazars, different colour-index combinations were obtained and plotted against the magnitude, popularly known as the color-magnitude diagram (CMD). In general, in the optical band most BL Lacs exhibit a bluer-when-brighter (BWB) trend (Vagnetti et al. 2003; Li et al. 2024), while FSRQs display a redder-when-brighter (RWB) trend (Gu et al. 2006; Negi et al. 2022). Color variations on hour time scales for five sources having more than four simultaneous FUV and NUV photometric observations were studied. To study the color trends quantitatively, the CMDs for all combinations were fitted with an unweighted linear least-squares fit of the form, color index (CI) = $m \times M + c$, where, M is the magnitude, and m and c are slope and intercept, respectively. A positive value of the slope indicates a BWB trend, while a negative value hints toward the presence of a RWB trend. For the trend to be significant at the 99% significance level, the correlation coefficient (R) is to be more than 0.5 (Prince et al. 2021). In addition to the unweighted least-squares fit to the points on the CMD, a weighted linear least-squares fit was also carried out by considering the errors in both the colors and the

Table 4. Results of variability analysis for sources showing variability. Here, N is the number of orbits and σ_m is the amplitude of flux variability in magnitude.

Name	Date	Filter	N	σ_m
	(dd-mm-yyyy)		(mag)	
PKS 0208–512	30-10-2016	F148W	4	0.06
1ES 0229+200	01-10-2017	N245M	3	0.03
	09-12-2017	F154W	4	0.12
	08-01-2018	F154W	4	0.04
		N245M	4	0.05
		F169M	11	0.03
OJ 287		N245M	7	0.01
	18-04-2018	F169M	24	0.03
	18-05-2020	F148W	6	0.01
		F154W	8	0.04
		F172M	10	0.04
		F148Wa	6	0.03
1ES 1101–232	30-12-2016	F154W	32	0.04
		N263M	32	0.03
1ES 1218+304	21-05-2016	F148W	13	0.01
H 1426+428	05-03-2018	F148W	8	0.03
		F154W	5	0.02
		N242W	4	0.03
		F172M	11	0.02
PKS 1510–089	16-03-2018	N219M	11	0.12
		F154W	4	0.02
PKS 2155–304	21-05-2018	F154W	3	0.02
	16-09-2019	F172M	3	0.98
1ES 2344+514	06-06-2017	F172M	3	0.98
	09-07-2017	F172M	3	0.06
		N245M	3	0.03
	07-09-2017	F172M	3	0.02
	07-12-2017	F172M	2	0.24

magnitudes. For this, a Bayesian linear regression with the LINMIX_ERR method (Kelly 2007) was used. This method is effective in handling errors in both the color and magnitude measurements as well as correlations between the errors. In addition to LINMIX_ERR, the Bivariate Correlated Errors and Intrinsic Scatter (BCES; Akritas & Bershady 1996) was also used, and the results are consistent with each other. For all the further discussions on spectral variability, the results from the Bayesian analysis are used.

4. RESULTS

4.1. Flux variability

All the ten blazar fields used in this work are less crowded. As the goal of the present study is to characterize the UV variability of blazars on hour-like time

scales, aperture photometry was carried out following the procedures outlined in Section 2. Of all the sources analyzed in this work, 9 sources were found to show flux variations, except that of Mrk 501, which was found to be non-variable. The results of the variability analysis for sources showing variability are given in Table 4, and the light curves generated for all the sample sources are given in Figs. 3 and 4. Further, details of the flux variability of each of the sources are given in Section 4.3.

4.2. Spectral variability

Flux variations in blazars are accompanied by spectral variations. The color changes in blazars on diverse time scales directly related to the spectrum of the blazar are well-studied by many authors in optical bands (Villata et al. 2004; Stalin et al. 2009; Bonning et al. 2012; Bhatta & Webb 2018; Gaur et al. 2019; Agarwal 2023), but genuine color behavior at different time scales is still one of the most puzzling issues in blazar physics. Moreover, color changes on hourly time scales in the UV bands are rarely studied in blazars, though few studies exist for Seyfert-type AGN (Chand et al. 2022). This is the first search for dominant color trends in blazars on the intraday time scale in the UV regime. A better understanding of dominant emission mechanisms in the source can be understood through the studies on spectral variations. The UV spectral variations can be contributed by both the accretion disk and the Doppler-boosted relativistic jets. In order to understand this, CMDs were generated for the sources. For this, the five sources which are variable and also having more than four simultaneous NUV and FUV measurements were only considered. The CMDs were then analyzed following the methodology described in Section 3.2. The fits to the CMDs of the sources are given in Fig. 5, and the results of the fit are given in Tables 5 and 6. BWB trend was observed for all the sources analysed for spectral variability. Studies in the literature (Villata et al. 2002; Raiteri et al. 2017) suggest that a BWB trend in blazars is due to intrinsic energetic processes in the jet.

4.3. Notes on individual sources

4.3.1. PKS 0208–512

PKS 0208–512 is a FSRQ of LSP type at a redshift of $z = 1.003$ (Healey et al. 2008). It has been detected by EGRET on board the *Compton Gamma Ray Observatory* (Hartman et al. 1999) and *Fermi* Gamma-Ray Space Telescope (Abdollahi et al. 2020). It has been studied for optical and infrared flux variations on a day-like time scale (Bonning et al. 2012). Between August 2008 and September 2011, the source underwent three optical and infrared bursts from monitoring observation

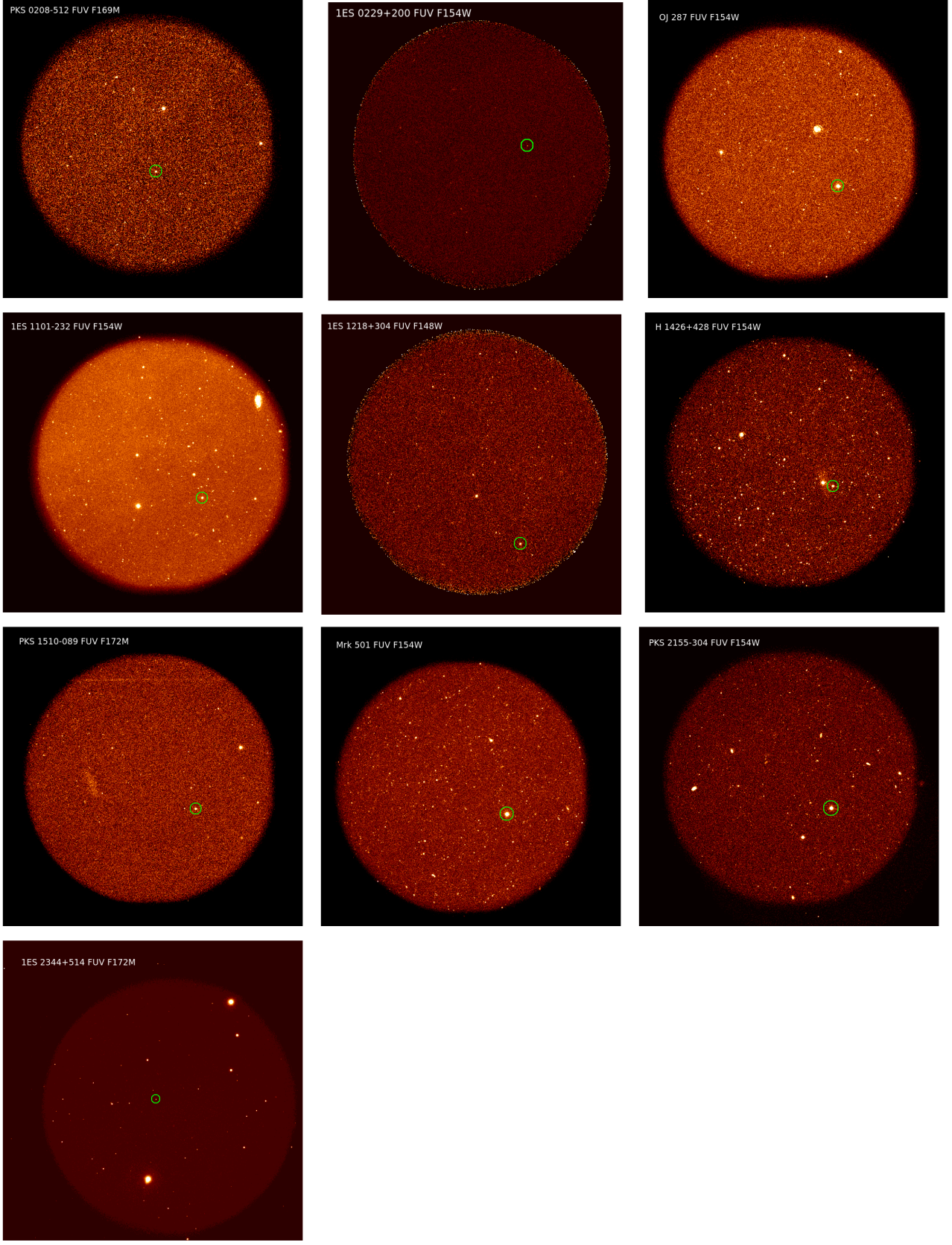


Figure 1. The observed FUV field images of the ten blazar sources. The target sources are shown in green circles. The source name and the corresponding filter name are given in each field image. Each image has a field of view of ~ 28 arcmin diameter.

Table 5. Results of unweighted linear least-squares fit to the colour magnitude diagram. Here, column 1 gives the name of the sources, column 2 gives the OBSID, column 3 gives the number of orbits used in the analysis, column 4 gives the FUV and NUV filters used to get the colour and brightness, column 5 gives the slope and the associated error, column 6 gives the intercept and the associated error, column 7 gives the linear correlation coefficient (R) and column 8 gives the probability of no correlation (P). The entries with 0 in P (column 6) indicates that the values are lesser than 1×10^{-2} .

Name	OBSID	No. of orbits	Color/Mag	Slope	Intercept	R	P
OJ 287	T01-163T01-9000001152	07	(F169M - N245M)/F169M	1.04 ± 0.20	-16.53 ± 3.34	0.92	0.00
1ES 1101–232	G06-086T02-9000000936	32	(F154W - N263M)/F154W	1.01 ± 0.12	-18.13 ± 2.20	0.84	0.00
1ES 1218+304	G05-211T01-9000000464	13	(F148W - N245M)/F148W	1.16 ± 0.14	-20.23 ± 2.46	0.93	0.00
H 1426+428	A04-094T01-9000001942	07	(F148W - N245M)/F148W	0.66 ± 0.38	-11.79 ± 7.16	0.61	0.15
PKS 1510–089	A04-101T01-9000001984	11	(F172M - N219M)/F172M	1.85 ± 0.58	-32.19 ± 10.03	0.73	0.01

Table 6. Results of fit to the points in the CMD using BCES and Bayesian methods. The columns have the meaning as given in Table 5.

Name	OBSID	No. of orbits	Color/Mag	BCES		Bayesian	
				Slope	Intercept	Slope	Intercept
OJ 287	T01-163T01-9000001152	07	(F169M - N245M)/F169M	1.08 ± 0.18	-17.18 ± 3.01	1.15 ± 1.02	-18.31 ± 16.74
1ES 1101–232	G06-086T02-9000000936	32	(F154W - N263M)/F154W	1.08 ± 0.17	-19.31 ± 3.19	1.29 ± 0.18	-23.35 ± 3.37
1ES 1218+304	G05-211T01-9000000464	13	(F148W - N245M)/F148W	1.04 ± 0.11	-18.14 ± 2.06	1.14 ± 0.54	-19.84 ± 9.70
H 1426+428	A04-094T01-9000001942	07	(F148W - N245M)/F148W	0.60 ± 0.32	-10.78 ± 5.97	1.07 ± 2.08	-19.50 ± 38.80
PKS 1510–089	A04-101T01-9000001984	11	(F172M - N219M)/F172M	2.75 ± 0.67	-47.89 ± 11.66	2.43 ± 1.74	-42.29 ± 30.10

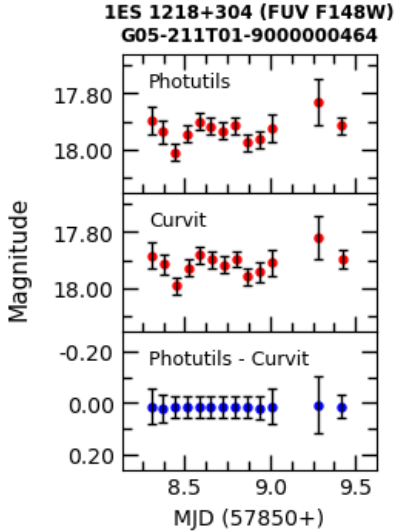


Figure 2. Comparison plot of FUV lightcurve for the source 1ES 1218+304 in F148W filter with top panel denoting *Photutils* lightcurve, middle panel denoting *Curvit* lightcurve, and bottom panel denoting the difference between *Photutils* and *Curvit* lightcurves.

on day-like time scales. Of the three optical infrared outbursts, only two outbursts and flares at GeV energies were observed. A RWB spectral variation was noticed in the optical and near-infrared bands (Chatterjee et al. 2013). It was found to show intra-night optical variability (Romero et al. 2002). Variations in the UV band are reported for the first time.

4.3.2. 1ES 0229+200

This is a very high energy γ -ray source (Aharonian et al. 2007a) and also detected in the GeV energy range by the *Fermi* Gamma-Ray Space Telescope (Ackermann et al. 2015). It was found to show optical flux variations within a night (Bachev et al. 2012) and on day-like time scales (Pandey et al. 2020) and VHE variations on month-like time scales (Cologna et al. 2015). It was also studied for X-ray flux variations in the 3–79 keV band using observations from *NuSTAR* (Pandey et al. 2017). It has not been studied for UV variations before. It was found to be variable on all the four epochs it was observed.

4.3.3. OJ 287

This source, believed to host a supermassive binary black hole (Sillanpaa et al. 1988), has been extensively studied for flux variations across wavelengths on a range of time scales, including UV (Bachev et al. 2012; Huang et al. 2022), optical (O'Dell et al. 1978) and GeV γ -rays (Agudo et al. 2011). In addition to flux variations, the source has also been studied for optical polariza-

tion variation (Rakshit et al. 2017). This source was observed for three epochs simultaneously in both FUV and NUV. The source was found to show variations on all three epochs. In addition to flux variations, the source was also found to show spectral variations in one of the epochs with a BWB trend.

4.3.4. 1ES 1101–232

This is a very high energy BL Lac (Aharonian et al. 2007b). It was found to show variations in the 3–79 keV band in X-rays (Pandey et al. 2018), optical flux (Romero et al. 2002) and polarization microvariability. This source has no previous record on its UV flux variations. This source was observed by UVIT on 30 December 2016, with two different filters (F154W and N263M). The source was found to show flux variations on hour-like time scale in both FUV and NUV bands. In addition to flux variability, the source was also found to show spectral variability with a BWB pattern.

4.3.5. 1ES 1218+304

It is an HSP blazar at a redshift $z = 0.182$ (Otero-Santos et al. 2022). It is also detected in GeV γ -rays by *Fermi* (Nolan et al. 2012) and in very high energy γ -rays from *MAGIC* (Albert et al. 2006) and from *VERITAS* (Acciari et al. 2009) observations. It has been studied for optical flux variations both in long-term (Negi et al. 2022) and within a night (Gopal-Krishna et al. 2011). It is highly polarized in the optical with a polarization degree of $6.83 \pm 0.70\%$ (Jannuzzi et al. 1994). It has been found to be variable in the X-ray band in the 0.3–10 keV energy range from *XMM-Newton* observations (Devanand et al. 2022), in the hard X-ray band from *NuSTAR* observations (Pandey et al. 2018) and in the high energy γ -ray band from *VERITAS* (Acciari et al. 2010). From *Swift*/UVOT observations 1ES 1218+304 was found to show long term variations in UV (Moo et al. 2022). However, it has not been studied for UV variations on hour-like time scales before. The source was observed on one epoch. On this epoch, the source was found to show flux variations as well as a BWB spectral variability.

4.3.6. H 1426+428

It is an extreme HSP blazar (Costamante et al. 2001) and was detected in TeV γ -rays from observations with the Whipple telescope (Horan et al. 2002) and from *HEGRA* observations (Aharonian et al. 2002). In the radio band, it has a compact core surrounded by a halo (Giroletti et al. 2004). From *VLBA* observations at 8 GHz, Piner et al. (2008) found the source to have a parsec scale radio structure consisting of a core and a single

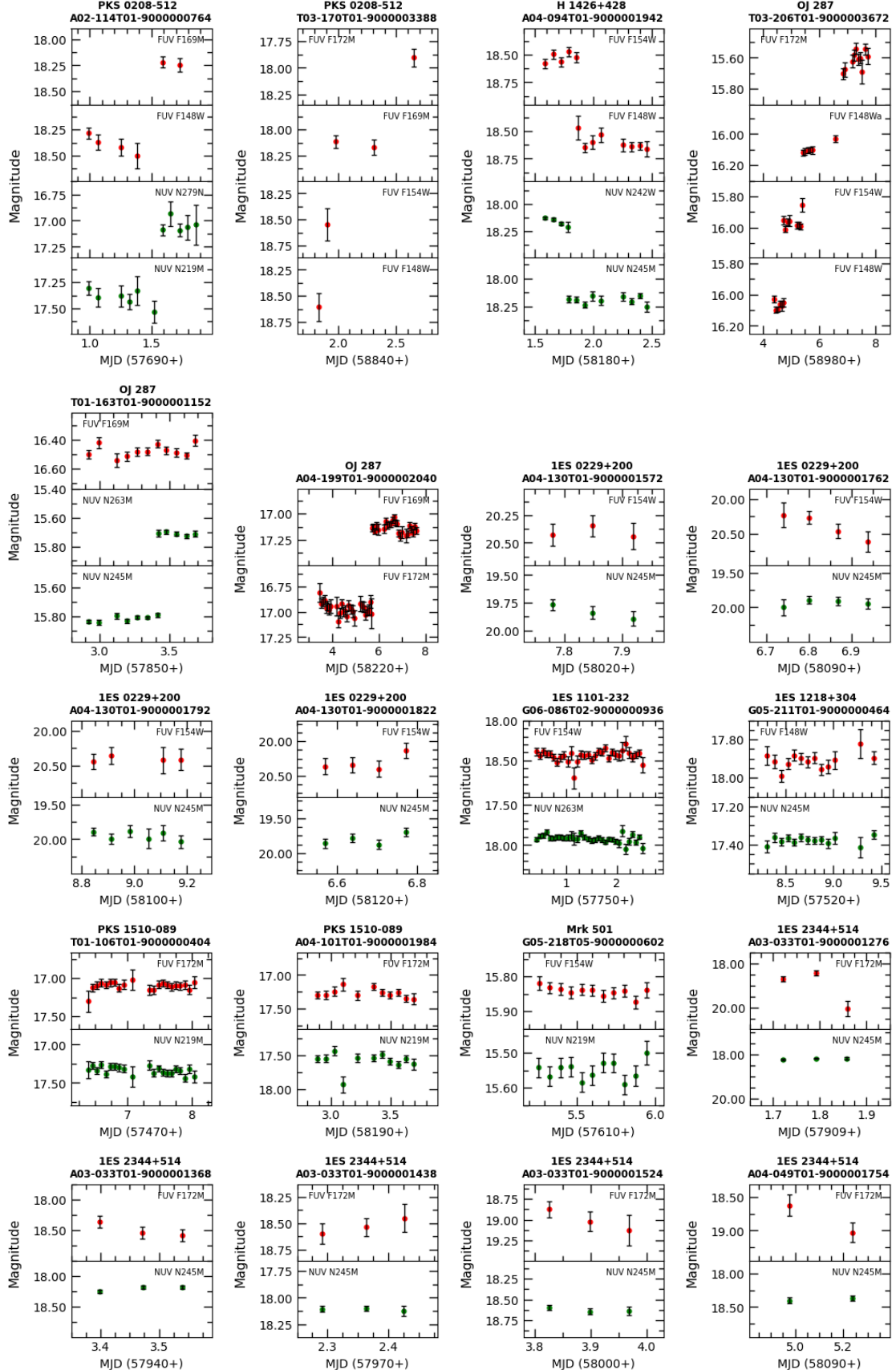


Figure 3. FUV and NUV light curves (represented by red and green color circles, respectively) of sources. The observation ID and source name are labeled in each plot. The name of the filters used for the light curves are given in each panel.

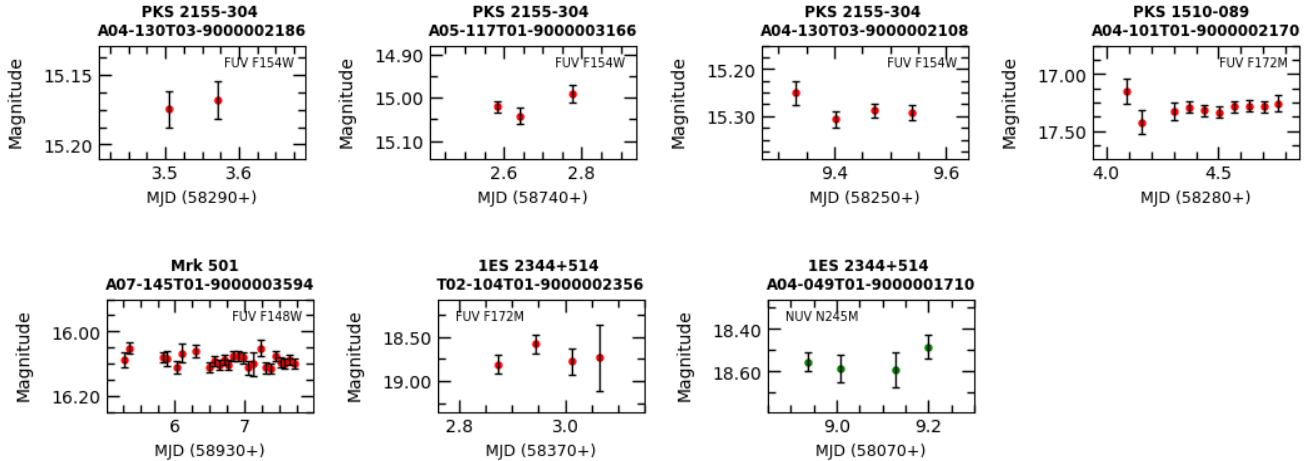


Figure 4. FUV and NUV light curves of sources. Here, red dots denote FUV light curves and green dots denote NUV light curves. The respective source name and observation ID are mentioned on top of each plot. Also, the names of the filters used for the light curves are given in each panel.

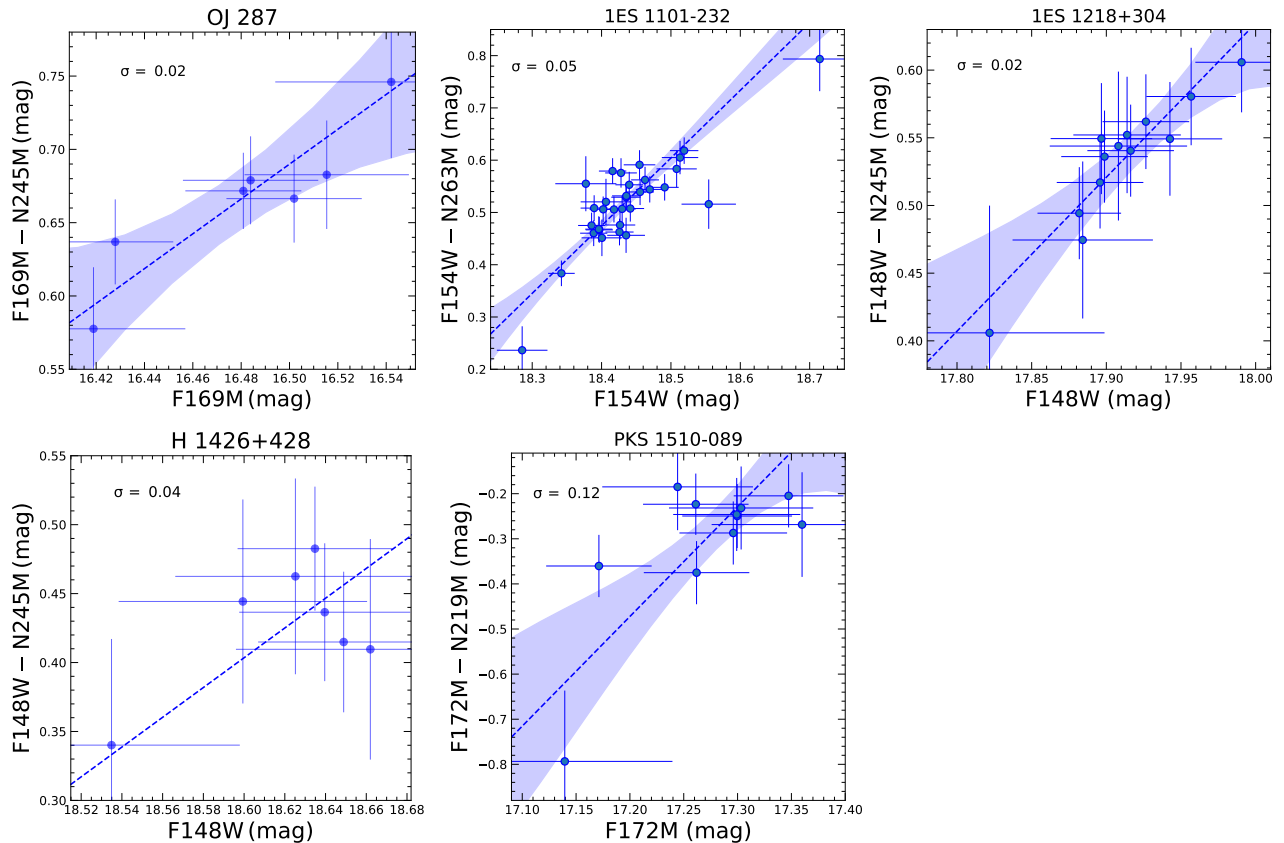


Figure 5. CMDs for the sources that are variable and having more than four simultaneous FUV and NUV photometric data points. The best fit line from Bayesian analysis using LINMIX.ERR is shown by the dashed blue line and the uncertainty range on the best fit is shown by the blue shaded region. The intrinsic scatter (σ) is given in the respective plots. The names of the sources are given on the top of each panel (see also Table 5 and 6).

jet component. It was observed to show optical flux variations within a night (Gopal-Krishna et al. 2011). It was found to show long-term flux and color variations in the optical (Gaur et al. 2012; Negi et al. 2022) as well as flux variation in X-rays (Devanand et al. 2022). It is polarized in the optical and also show polarization variations (Hovatta et al. 2016). This source has been studied for UV flux variations for the first time. The source was found to show both flux and spectral variations (BWB trend) on the single epoch it was observed.

4.3.7. PKS 1510–089

It is an FSRQ at $z = 0.360$ (Thompson et al. 1990) and powered by a black hole of mass $5.7_{-0.58}^{+0.62} \times 10^7 M_\odot$ (Rakshit 2020). It is known to emit high energy γ -rays in GeV band and also in TeV from HESS (H. E. S. S. Collaboration et al. 2013) and MAGIC (MAGIC Collaboration et al. 2018). Quasi-periodic oscillation (QPO) was detected in the GeV light curve of the source (Roy et al. 2022). PKS 1510–089 has been studied for correlation between flux variations between different wavelengths. The flux variations in the γ -ray and optical/IR bands were found to precede the variations in the radio band (Yuan et al. 2023). While Ramakrishnan et al. (2016) found the long-term optical and γ -ray flux variations to be correlated with zero lag, Rajput et al. (2020) found complex flux variability behavior between optical and γ -ray bands. In the broad band SED, optical/UV emission was found to be dominated by emission from the accretion disk (Barnacka et al. 2014). It was known to show short time scale flux variations in the optical (Gopal-Krishna et al. 2011; Romero et al. 1999, 2002) and γ -rays (Saito et al. 2013). It is polarized in the optical and also shows polarization variations (Andruchow et al. 2005). From observations carried out with IUE, the source was found to show variability in the UV continuum (Obrien et al. 1988). This source has not been studied before for short-term variations in the UV. This source was detected in three epochs. It was found to show flux and spectral variability in one of the epochs.

4.3.8. Mrk 501

This nearby source ($z = 0.034$) is a strong X-ray and TeV γ -ray source (Pian et al. 1998; Djannati-Atai et al. 1999) with a black hole of mass $10^{8.93 \pm 0.21} M_\odot$ (Falomo et al. 2002). In the radio band, at the parsec scale, the source is known to have a relativistically boosted one-sided jet (Edwards & Piner 2002). It is known to be variable in X-rays and TeV γ -rays (Gliozzi et al. 2006). In the optical, rapid variations on the time scale of minutes have been observed (Zeng et al. 2019). In addition to flux variations, optical color variations have also been observed. This source was observed for two epochs

to know their UV variability nature on hour-like time scales. On both epochs, it was found that the source does not show any variability.

4.3.9. PKS 2155–304

This HSP blazar situated at $z = 0.116$ (Falomo et al. 1993) has been extensively studied across wavelengths. It is variable in the optical (Gaur et al. 2010; Romero et al. 1999), X-rays (Zhang et al. 2021), γ -rays (Rieger & Volpe 2010), UV from observations with the IUE (Urry et al. 1993) and in the extreme UV from the Extreme Ultraviolet Explorer observations (Marshall et al. 2001). QPO has been detected in the optical (Sandrinelli et al. 2014), X-ray (Lachowicz et al. 2009) and GeV γ -rays (Ren et al. 2023). It is polarized in the optical and also shows polarization variations (Peceur et al. 2020). This source was observed for three epochs in the FUV band, and on all the occasions, it was found to be variable.

4.3.10. 1ES 2344+514

The source 1ES 2344+514 at a redshift of $z = 0.044$ (Perlman et al. 1996) is an X-ray source detected in the Einstein Slew Survey (Elvis et al. 1992) and is also a VHE γ -ray emitter (Catanese et al. 1998). It is also detected by VERITAS (Acciari et al. 2011) and MAGIC (MAGIC Collaboration et al. 2020). It was found to have short time scale variation in X-rays (Giommi et al. 2000) and optical (Pandey et al. 2020). In the optical, it was also found to show variations on day-like time scales (Dai et al. 2001; Gaur et al. 2012; Cai et al. 2022). It is also variable in γ -rays (Grube 2008). On long-time scales, it is found to be variable in UV based on observations with the Swift/UVOT acquired over a period of three years from 2019 to 2021 (Abe & et al. 2024). This source has been observed for seven epochs to know its UV variability nature on hour-like time scale. The source was found to show flux variability on four epochs.

5. DISCUSSION AND CONCLUSIONS

Flux variability in blazars in UV is found to be extremely useful for getting insights into the inner region close to the SMBH, radiation mechanisms taking place in the vicinity of SMBH, and the relativistic jets. However, because intranight observations using space-based UV telescopes are time-expensive, the nature of UV variability in blazars is not well-studied in the literature. Recently, several studies have been conducted on large samples of optically selected quasars using their UV data obtained with *GALEX* (Punsly et al. 2016, 2021) and covering a day or longer timescales. Here, the first study was performed to explore the properties of blazars in UV on the shorter, hour-like time scales. For this purpose, a sample of 10 blazars was concentrated, comprising of 2

FSRQs and 8 BL Lacs objects that were observed using UVIT payload onboard *AstroSat*.

In blazars, the UV emission obtained by the instrument is widely believed to be non-thermal synchrotron emission along the jet axis. Doppler factor δ is defined as $\delta = 1/\Gamma(1 - \beta \cos \theta_{obs})$, where Γ is the bulk Lorentz factor, β is the speed of emission region in the units of speed of light, and θ_{obs} is the angle of the jet with respect to the line of sight to the observer. In blazars, the observer's line of sight is closely aligned with the orientation of the relativistic jet (Urry & Padovani 1995), and thus, the jet emission undergoes Doppler boosting owing to a higher apparent Lorentz factor, and thus, the jet emission overpowers the thermal radiation from the accretion disc. This is followed by a series of effects, such as amplified flux and blueshifted emitted frequencies, which causes the shortening of their apparent variability time scales (Urry & Padovani 1995). Because of the above reasons, blazar variability is an excellent tool for shedding light on the structure of jets and understanding the emission mechanisms taking place in them.

Various theoretical models used to explain blazar variability are broadly divided into extrinsic and intrinsic mechanisms. The probable intrinsic mechanisms include shocks traveling down the jet or magnetic irregularities or accretion disc instabilities (Blandford & Königl 1979; Marscher et al. 2008; Mohan & Mangalam 2015, and references therein). Whereas the extrinsic effects involve interstellar scintillation as well as variations in the viewing angle leading to changes in the Doppler factor, or gravitational microlensing (Schneider & Weiss 1987, and references therein). During the low state in blazars, UV variability can be attributed to the instabilities or hot spots on the accretion disk (Chakrabarti & Wiita 1993). However, various multi-wavelength studies of these sources have demonstrated that the electromagnetic emission from all these blazars is jet-dominated (Barnacka et al. 2014; Sahakyan 2020; Prince et al. 2021a; Kushwaha et al. 2021; Prince et al. 2021b; Diwan et al. 2023; Goswami et al. 2024). Therefore, it is tempting to postulate that the observed variable UV emission from them could be largely contributed by their Doppler boosted relativistic jet. To further investigate this claim, we analysed the colour-magnitude relationship of the sample sources.

Blazars, a subclass of AGN, exhibit intriguing color or spectral index variations that play a crucial role in unraveling their underlying emission mechanisms. These enigmatic cosmic objects exhibit various behaviors in their CMDs. CMDs of blazars have shown to exhibit three distinct trends namely, RWB, BWB and achro-

matic behaviours. Generally, most studies indicate that BWB chromatism is the dominant behavior in most of the BL Lac objects, while RWB chromatism is typical of FSRQs (Vagnetti et al. 2003; Agarwal et al. 2022, 2023, and references therein). However, the color-magnitude correlation in blazars still remains a topic of debate in literature. The BWB trend is often explained by a single-component synchrotron model where an influx of freshly injected electrons with a harder energy distribution than the previous cooler electrons leads to increased flux and a bluer spectrum. Also, electrons accelerated at the shock front have higher energies, they gradually lose energy due to radiative cooling, thereby showing more variations at the higher energy band (Kirk et al. 1998; Mastichiadis & Kirk 2002). Existence of an energy stratified jet also finds support from the energy dependent polarization observed recently in HSP blazars such as Mrk 421 (Kim et al. 2024) and 1ES 0229+200 (Ehlerl et al. 2023). Furthermore, this trend can also be elucidated by a two-component emission model. In this scenario, a stable component with a constant spectral index ($\alpha_{constant}$) coexists with a variable component characterized by a flatter slope (α_1). As the variable component outshines the stable one, chromatic behaviors emerge, influencing short-term behavior (dominated by pronounced chromatic components) and longer-term variations (attributed to a mildly chromatic component). In all the sources studied for spectral variations, a BWB behavior was found, also suggesting that the variable flux seen in the sample sources could be attributed to synchrotron emission from the jet, potentially signaling an enhancement in particle acceleration efficiency. One of the FSRQs, namely PKS 1510–089, also displayed the BWB trend, thus suggesting that the jets of BL Lacs and FSRQs could be fundamentally the same.

Detailed spectral measurements of a handful of blazar jets based on examination of flux densities of the knots in the kiloparsec-scale jets hint towards the fact that a significant portion of their synchrotron UV radiation might come from relativistic particles different from those responsible for optical/IR emission. The study displays an increase toward the UV and a smooth transition to X-ray data points, thus revealing a clear spectral upturn in the optical/UV region of their spectral energy distributions (Uchiyama et al. 2006). The presence of high polarization in the UV emission, as found by Cara et al. (2013), supports the origin of this high energy component. The above findings have also been confirmed by Chand et al. (2022) by studying the optical and UV emissions (rest-frame) from blazars.

The scarcity of information on the UV variability in blazars is due to the expensive nature of carrying out intranight monitoring campaigns using space-based UV telescopes (Smith et al. 2018). To tackle this challenge, recent efforts have leveraged UV data collected by *GALEX* for large samples of AGN. However, these studies mainly focused on day-long or longer time scales monitoring of the optically selected quasars (Punsly et al. 2016), thereby examining the accretion disc rather than the relativistic jet of these sources. To delve into the rapid UV variability of blazars, UV flux variability characteristics on hourly time scales of 10 blazars observed using UVIT on board *AstroSat* in FUV and NUV filters were studied. UV flux variations on time scales of hours was found in 9 blazars. Also, the color-magnitude relationship was analyzed for the sample of sources that are found to be variable and having more than 4 simultaneous observations in FUV and NUV filters namely OJ 287, 1ES 1101–232, 1ES 1218+304, H 1426+428 and PKS 1510–089. Of these the first four sources belong to the BL Lac category, while PKS 1510–089 is a FSRQ. Thus, both FSRQs and BL Lacs in the sample were

found to display a dominant BWB chromatism in the UV region. The above findings indicate the dominance of the synchrotron emission from the Doppler-boosted jet for this sample of blazars in UV band.

ACKNOWLEDGEMENTS

The authors extend their sincere gratitude to the anonymous reviewer for the useful comments and suggestions on the manuscript. This research made use of Photutils, an Astropy package for detection and photometry of astronomical sources (Bradley et al. 2023). This publication uses the data from the *AstroSat* mission of the Indian Space Research Organisation (ISRO), archived at the Indian Space Science Data Centre (ISSDC). This publication uses UVIT data processed by the payload operations centre at Indian Institute of Astrophysics (IIA), Bangalore. The UVIT is built in collaboration between IIA, Inter University Center for Astronomy and Astrophysics (IUCAA), Tata Institute of Fundamental Research (TIFR), ISRO and Canadian Space Agency (CSA). One of the authors (SBG) thanks the IUCAA, Pune, India for the Visiting Associateship.

REFERENCES

- Abdo, A. A., Ackermann, M., Agudo, I., et al. 2010, ApJ, 716, 30, doi: [10.1088/0004-637X/716/1/30](https://doi.org/10.1088/0004-637X/716/1/30)
- Abdo, A. A., Ackermann, M., Ajello, M., et al. 2011, The Astrophysical Journal, 736, 131
- Abdollahi, S., Acero, F., Ackermann, M., et al. 2020, ApJS, 247, 33, doi: [10.3847/1538-4365/ab6bcb](https://doi.org/10.3847/1538-4365/ab6bcb)
- Abe, T., & et al. 2024, A&A, 682, A114, doi: [10.1051/0004-6361/202345678](https://doi.org/10.1051/0004-6361/202345678)
- Acciari, V. A., Aliu, E., Arlen, T., et al. 2009, ApJ, 695, 1370, doi: [10.1088/0004-637X/695/2/1370](https://doi.org/10.1088/0004-637X/695/2/1370)
- Acciari, V. A., Aliu, E., Beilicke, M., et al. 2010, ApJL, 709, L163, doi: [10.1088/2041-8205/709/2/L163](https://doi.org/10.1088/2041-8205/709/2/L163)
- Acciari, V. A., Aliu, E., Arlen, T., et al. 2011, Astrophysical Journal, 738, 169, doi: [10.1088/0004-637X/738/2/169](https://doi.org/10.1088/0004-637X/738/2/169)
- Ackermann, M., Ajello, M., Atwood, W. B., et al. 2015, ApJ, 810, 14, doi: [10.1088/0004-637X/810/1/14](https://doi.org/10.1088/0004-637X/810/1/14)
- Agarwal, A. 2023, ApJ, 946, 109, doi: [10.3847/1538-4357/acbdfa](https://doi.org/10.3847/1538-4357/acbdfa)
- Agarwal, A., Pandey, A., Özdonmez, A., et al. 2022, ApJ, 933, 42, doi: [10.3847/1538-4357/ac6cef](https://doi.org/10.3847/1538-4357/ac6cef)
- Agarwal, A., Mihov, B., Agrawal, V., et al. 2023, ApJS, 265, 51, doi: [10.3847/1538-4365/acbcdb](https://doi.org/10.3847/1538-4365/acbcdb)
- Agrawal, P. C. 2017, Journal of Astrophysics and Astronomy, 38, 27, doi: [10.1007/s12036-017-9449-6](https://doi.org/10.1007/s12036-017-9449-6)
- Agudo, I., Jorstad, S. G., Marscher, A. P., et al. 2011, ApJL, 726, L13, doi: [10.1088/2041-8205/726/1/L13](https://doi.org/10.1088/2041-8205/726/1/L13)
- Aharonian, F., Akhperjanian, A., Barrio, J., et al. 2002, A&A, 384, L23, doi: [10.1051/0004-6361:20020206](https://doi.org/10.1051/0004-6361:20020206)
- Aharonian, F., Akhperjanian, A. G., Barres de Almeida, U., et al. 2007a, A&A, 475, L9, doi: [10.1051/0004-6361:20078462](https://doi.org/10.1051/0004-6361:20078462)
- Aharonian, F., Akhperjanian, A. G., Bazer-Bachi, A. R., et al. 2007b, A&A, 470, 475, doi: [10.1051/0004-6361:20077057](https://doi.org/10.1051/0004-6361:20077057)
- Ai, Y. L., Yuan, W., Zhou, H. Y., et al. 2010, ApJL, 716, L31, doi: [10.1088/2041-8205/716/1/L31](https://doi.org/10.1088/2041-8205/716/1/L31)
- Akritas, M. G., & Bershady, M. A. 1996, The Astrophysical Journal, 470, 706, doi: [10.1086/177901](https://doi.org/10.1086/177901)
- Albert, J., Aliu, E., Anderhub, H., et al. 2006, ApJL, 642, L119, doi: [10.1086/504845](https://doi.org/10.1086/504845)
- Andruchow, I., Romero, G. E., & Cellone, S. A. 2005, A&A, 442, 97, doi: [10.1051/0004-6361:20053325](https://doi.org/10.1051/0004-6361:20053325)
- Angel, J. R. P., & Stockman, H. S. 1980, ARA&A, 18, 321, doi: [10.1146/annurev.aa.18.090180.001541](https://doi.org/10.1146/annurev.aa.18.090180.001541)
- Antonucci, R. 1993, ARA&A, 31, 473, doi: [10.1146/annurev.aa.31.090193.002353](https://doi.org/10.1146/annurev.aa.31.090193.002353)
- Bachev, R., Semkov, E., Strigachev, A., et al. 2012, MNRAS, 424, 2625, doi: [10.1111/j.1365-2966.2012.21310.x](https://doi.org/10.1111/j.1365-2966.2012.21310.x)
- Barnacka, A., Moderski, R., Behera, B., Brun, P., & Wagner, S. 2014, Astronomy & Astrophysics, 567, A113

- Bhatta, G., & Webb, J. 2018, *Galaxies*, 6, 2, doi: [10.3390/galaxies6010002](https://doi.org/10.3390/galaxies6010002)
- Blandford, R. D., & Königl, A. 1979, *ApJ*, 232, 34, doi: [10.1086/157262](https://doi.org/10.1086/157262)
- Blandford, R. D., & Rees, M. J. 1978, *PhyS*, 17, 265, doi: [10.1088/0031-8949/17/3/020](https://doi.org/10.1088/0031-8949/17/3/020)
- Bonning, E., Urry, C. M., Bailyn, C., et al. 2012, *ApJ*, 756, 13, doi: [10.1088/0004-637X/756/1/13](https://doi.org/10.1088/0004-637X/756/1/13)
- Bonnoli, G., Ghisellini, G., Foschini, L., Tavecchio, F., & Ghirlanda, G. 2011, *Monthly Notices of the Royal Astronomical Society*, 410, 368
- Bradley, L., Sipócz, B., Robitaille, T., et al. 2023, *astropy/photutils*: 1.12.0, 1.10.0, Zenodo, doi: [10.5281/zenodo.1035865](https://doi.org/10.5281/zenodo.1035865)
- Cai, Z.-Y., Wu, X.-B., Yang, J., et al. 2022, *ApJS*, 260, 47, doi: [10.3847/1538-4365/ac7cd3](https://doi.org/10.3847/1538-4365/ac7cd3)
- Cara, M., Perlman, E. S., Uchiyama, Y., et al. 2013, *ApJ*, 773, 186, doi: [10.1088/0004-637X/773/2/186](https://doi.org/10.1088/0004-637X/773/2/186)
- Catanese, M., Akerlof, C. W., Badran, H. M., et al. 1998, *ApJ*, 501, 616, doi: [10.1086/305831](https://doi.org/10.1086/305831)
- Chakrabarti, S. K., & Wiita, P. J. 1993, *A&A*, 271, 216
- Chand, K., Gopal-Krishna, Omar, A., et al. 2022, *MNRAS*, 511, 13, doi: [10.1093/mnrasl/slab129](https://doi.org/10.1093/mnrasl/slab129)
- Chatterjee, R., Fossati, G., Urry, C. M., et al. 2013, *ApJL*, 763, L11, doi: [10.1088/2041-8205/763/1/L11](https://doi.org/10.1088/2041-8205/763/1/L11)
- Cologna, G., Mohamed, M., Wagner, S., et al. 2015, in *International Cosmic Ray Conference*, Vol. 34, 34th International Cosmic Ray Conference (ICRC2015), 762, doi: [10.22323/1.236.0762](https://doi.org/10.22323/1.236.0762)
- Costamante, L., Ghisellini, G., Giommi, P., et al. 2001, *A&A*, 371, 512, doi: [10.1051/0004-6361:20010412](https://doi.org/10.1051/0004-6361:20010412)
- Dai, X., Zhang, B., Gou, L., & Mészáros, P. 2001, *AJ*, 122, 2901, doi: [10.1086/324103](https://doi.org/10.1086/324103)
- Devanand, P. U., Gupta, A. C., Jithesh, V., & Wiita, P. J. 2022, *ApJ*, 939, 80, doi: [10.3847/1538-4357/ac9064](https://doi.org/10.3847/1538-4357/ac9064)
- Diwan, R., Prince, R., Agarwal, A., et al. 2023, *Monthly Notices of the Royal Astronomical Society*, 524, 4333
- Djannati-Atai , A., Piron, F., Barrau, A., et al. 1999, *A&A*, 350, 17, doi: [10.48550/arXiv.astro-ph/9906060](https://doi.org/10.48550/arXiv.astro-ph/9906060)
- Edelson, R. 1992, *ApJ*, 401, 516, doi: [10.1086/172083](https://doi.org/10.1086/172083)
- Edwards, P. G., & Piner, B. G. 2002, *ApJL*, 579, L67, doi: [10.1086/345290](https://doi.org/10.1086/345290)
- Ehlert, S. R., Liidakis, I., Middei, R., et al. 2023, *The Astrophysical Journal*, 959, 61
- Elvis, M., Plummer, D., Schachter, J., & Fabbiano, G. 1992, *ApJS*, 80, 257, doi: [10.1086/191700](https://doi.org/10.1086/191700)
- Falomo, R., Kotilainen, J. K., & Treves, A. 2002, *ApJL*, 569, L35, doi: [10.1086/340642](https://doi.org/10.1086/340642)
- Falomo, R., Pesce, J. E., & Treves, A. 1993, *ApJL*, 411, L63, doi: [10.1086/186913](https://doi.org/10.1086/186913)
- Gaur, H., Gupta, A. C., Lachowicz, P., & Wiita, P. J. 2010, *ApJ*, 718, 279, doi: [10.1088/0004-637X/718/1/279](https://doi.org/10.1088/0004-637X/718/1/279)
- Gaur, H., Gupta, A. C., Wiita, P. J., Joshi, U. C., & Bai, J. M. 2012, *MNRAS*, 420, 3147, doi: [10.1111/j.1365-2966.2011.20234.x](https://doi.org/10.1111/j.1365-2966.2011.20234.x)
- Gaur, H., Gupta, A. C., Strigachev, A., et al. 2012, *MNRAS*, 425, 3002, doi: [10.1111/j.1365-2966.2012.21583.x](https://doi.org/10.1111/j.1365-2966.2012.21583.x)
- Gaur, H., Gupta, A. C., Bachev, R., et al. 2019, *MNRAS*, 484, 5633, doi: [10.1093/mnras/stz322](https://doi.org/10.1093/mnras/stz322)
- Ghisellini, G., Tavecchio, F., Foschini, L., & Ghirlanda, G. 2011, *MNRAS*, 414, 2674, doi: [10.1111/j.1365-2966.2011.18578.x](https://doi.org/10.1111/j.1365-2966.2011.18578.x)
- Ghosh, S. K., Tandon, S. N., Joseph, P., et al. 2021, *Journal of Astrophysics and Astronomy*, 42, 29, doi: [10.1007/s12036-020-09686-z](https://doi.org/10.1007/s12036-020-09686-z)
- Ghosh, S. K., Tandon, S. N., Singh, S. K., et al. 2022, *Journal of Astrophysics and Astronomy*, 43, 77, doi: [10.1007/s12036-022-09842-7](https://doi.org/10.1007/s12036-022-09842-7)
- Giommi, P., Perri, M., & Fiore, F. 2000, *MNRAS*, 317, 743, doi: [10.1046/j.1365-8711.2000.03599.x](https://doi.org/10.1046/j.1365-8711.2000.03599.x)
- Giroletti, M., Giovannini, G., Taylor, G. B., & Falomo, R. 2004, *ApJ*, 613, 752, doi: [10.1086/423231](https://doi.org/10.1086/423231)
- Gliozzi, M., Sambruna, R. M., Jung, I., et al. 2006, *ApJ*, 646, 61, doi: [10.1086/504700](https://doi.org/10.1086/504700)
- Gopal-Krishna, Goyal, A., Joshi, S., et al. 2011, *MNRAS*, 416, 101, doi: [10.1111/j.1365-2966.2011.19014.x](https://doi.org/10.1111/j.1365-2966.2011.19014.x)
- Goswami, P., Zacharias, M., Zech, A., et al. 2024, *Astronomy & Astrophysics*, 682, A134
- Grube, J. 2008, in *American Institute of Physics Conference Series*, Vol. 1085 (AIP), 662–665, doi: [10.1063/1.3076751](https://doi.org/10.1063/1.3076751)
- Gu, M., Lee, C.-U., Pak, S., Yim, H., & Fletcher, A. 2006, *Astronomy & Astrophysics*, 450, 39
- H.E. S. S. Collaboration, Abramowski, A., Acero, F., et al. 2013, *A&A*, 554, A107, doi: [10.1051/0004-6361/201321135](https://doi.org/10.1051/0004-6361/201321135)
- Hartman, R. C., Bertsch, D. L., Bloom, S. D., et al. 1999, *ApJS*, 123, 79, doi: [10.1086/313231](https://doi.org/10.1086/313231)
- Healey, S. E., Romani, R. W., Cotter, G., et al. 2008, *ApJS*, 175, 97, doi: [10.1086/523302](https://doi.org/10.1086/523302)
- Horan, D., Badran, H. M., Bond, I. H., et al. 2002, *ApJ*, 571, 753, doi: [10.1086/340019](https://doi.org/10.1086/340019)
- Hovatta, T., Lindfors, E., Blinov, D., et al. 2016, *A&A*, 596, A78, doi: [10.1051/0004-6361/201628974](https://doi.org/10.1051/0004-6361/201628974)
- Huang, S., Hu, S., Yin, H., et al. 2022, *MNRAS*, 515, 2778, doi: [10.1093/mnras/stac2022](https://doi.org/10.1093/mnras/stac2022)
- Jannuzzi, B. T., Smith, P. S., & Elston, R. 1994, *ApJ*, 428, 130, doi: [10.1086/174226](https://doi.org/10.1086/174226)

- Joseph, P., Stalin, C. S., Tandon, S. N., & Ghosh, S. K. 2021, Journal of Astrophysics and Astronomy, 42, 25, doi: [10.1007/s12036-020-09680-5](https://doi.org/10.1007/s12036-020-09680-5)
- Kelly, B. C. 2007, The Astrophysical Journal, 665, 1489, doi: [10.1086/519947](https://doi.org/10.1086/519947)
- Kim, D. E., Di Gesu, L., Liodakis, I., et al. 2024, Astronomy & Astrophysics, 681, A12
- Kirk, J. G., Rieger, F. M., & Mastichiadis, A. 1998, A&A, 333, 452. <https://arxiv.org/abs/astro-ph/9801265>
- Kushwaha, P., Singh, K. P., Sinha, A., et al. 2021, arXiv preprint arXiv:2107.10783
- Lachowicz, P., Gupta, A. C., Gaur, H., & Wiita, P. J. 2009, A&A, 506, L17, doi: [10.1051/0004-6361/200913161](https://doi.org/10.1051/0004-6361/200913161)
- Li, H.-Z., Guo, D.-F., Qin, L.-H., et al. 2024, Monthly Notices of the Royal Astronomical Society, 528, 6823
- Lynden-Bell, D. 1969, Nature, 223, 690, doi: [10.1038/223690a0](https://doi.org/10.1038/223690a0)
- MAGIC Collaboration, Acciari, V. A., Ansoldi, S., et al. 2018, A&A, 619, A159, doi: [10.1051/0004-6361/201833618](https://doi.org/10.1051/0004-6361/201833618)
- MAGIC Collaboration, et al. 2020, MNRAS, 496, 3912, doi: [10.1093/mnras/staa1676](https://doi.org/10.1093/mnras/staa1676)
- Marscher, A. P., Jorstad, S. G., D'Arcangelo, F. D., et al. 2008, Nature, 452, 966, doi: [10.1038/nature06895](https://doi.org/10.1038/nature06895)
- Marshall, H. L., Urry, C. M., Sambruna, R. M., & Pesce, J. E. 2001, ApJ, 549, 938, doi: [10.1086/319461](https://doi.org/10.1086/319461)
- Mastichiadis, A., & Kirk, J. G. 2002, Publications of the Astronomical Society of Australia, 19, 138
- Mohan, P., & Mangalam, A. 2015, ApJ, 805, 91, doi: [10.1088/0004-637X/805/2/91](https://doi.org/10.1088/0004-637X/805/2/91)
- Moo, K. E., Bregman, J. N., & Reynolds, M. T. 2022, ApJ, 931, 83, doi: [10.3847/1538-4357/ac5ea5](https://doi.org/10.3847/1538-4357/ac5ea5)
- Negi, V., Joshi, R., Chand, K., et al. 2022, Monthly Notices of the Royal Astronomical Society, 510, 1791
- Negi, V., Joshi, R., Chand, K., et al. 2022, MNRAS, 510, 1791, doi: [10.1093/mnras/stab3591](https://doi.org/10.1093/mnras/stab3591)
- Nolan, P. L., Abdo, A. A., Ackermann, M., et al. 2012, ApJS, 199, 31, doi: [10.1088/0067-0049/199/2/31](https://doi.org/10.1088/0067-0049/199/2/31)
- Obrien, P. T., Gondhalekar, P. M., & Wilson, R. 1988, in ESA Special Publication, Vol. 2, ESA Special Publication, ed. N. Longdon & E. J. Rolfe, 261–264
- O'Dell, S. L., Puschell, J. J., Stein, W. A., & Warner, J. W. 1978, ApJS, 38, 267, doi: [10.1086/190557](https://doi.org/10.1086/190557)
- Otero-Santos, J., Acosta-Pulido, J. A., Becerra González, J., et al. 2022, MNRAS, 511, 5611, doi: [10.1093/mnras/stac475](https://doi.org/10.1093/mnras/stac475)
- Paliya, V. S., Marcotulli, L., Ajello, M., et al. 2017, The Astrophysical Journal, 851, 33
- Paliya, V. S., Parker, M., Fabian, A., & Stalin, C. 2016, The Astrophysical Journal, 825, 74
- Paliya, V. S., Sahayanathan, S., & Stalin, C. 2015, The Astrophysical Journal, 803, 15
- Pandey, A., Gupta, A. C., Damljanovic, G., et al. 2020, MNRAS, 496, 1430, doi: [10.1093/mnras/staa1598](https://doi.org/10.1093/mnras/staa1598)
- Pandey, A., Gupta, A. C., & Wiita, P. J. 2017, ApJ, 841, 123, doi: [10.3847/1538-4357/aa705e](https://doi.org/10.3847/1538-4357/aa705e)
- . 2018, ApJ, 859, 49, doi: [10.3847/1538-4357/aabc5b](https://doi.org/10.3847/1538-4357/aabc5b)
- Pandey, A., Rajput, B., & Stalin, C. S. 2022, MNRAS, 510, 1809, doi: [10.1093/mnras/stab3338](https://doi.org/10.1093/mnras/stab3338)
- Pandey, S. B., Gupta, A. C., & Wiita, P. J. 2020, MNRAS, 496, 1430, doi: [10.1093/mnras/staa1664](https://doi.org/10.1093/mnras/staa1664)
- Peceur, N. W., Taylor, A. R., & Kraan-Korteweg, R. C. 2020, MNRAS, 495, 2162, doi: [10.1093/mnras/staa1333](https://doi.org/10.1093/mnras/staa1333)
- Perlman, E. S., Stocke, J. T., Schachter, J. F., et al. 1996, ApJS, 104, 251, doi: [10.1086/192315](https://doi.org/10.1086/192315)
- Pian, E., Vacanti, G., Tagliaferri, G., et al. 1998, ApJL, 492, L17, doi: [10.1086/311083](https://doi.org/10.1086/311083)
- Piner, B. G., Pant, N., & Edwards, P. G. 2008, ApJ, 678, 64, doi: [10.1086/533521](https://doi.org/10.1086/533521)
- Prince, R., Agarwal, A., Gupta, N., et al. 2021, A&A, 654, A38, doi: [10.1051/0004-6361/202140708](https://doi.org/10.1051/0004-6361/202140708)
- Prince, R., Agarwal, A., Gupta, N., et al. 2021a, Astronomy & Astrophysics, 654, A38
- Prince, R., Raman, G., Khatoon, R., et al. 2021b, Monthly Notices of the Royal Astronomical Society, 508, 315
- Punsly, B., Frey, S., Reynolds, C., et al. 2021, ApJ, 919, 40, doi: [10.3847/1538-4357/ac1070](https://doi.org/10.3847/1538-4357/ac1070)
- Punsly, B., Marziani, P., Zhang, S., Muzahid, S., & O'Dea, C. P. 2016, ApJ, 830, 104, doi: [10.3847/0004-637X/830/2/104](https://doi.org/10.3847/0004-637X/830/2/104)
- Raiteri, C. M., Villata, M., Acosta-Pulido, J. A., et al. 2017, Nature, 552, 374, doi: [10.1038/nature24623](https://doi.org/10.1038/nature24623)
- Rajput, B., Pandey, A., Stalin, C. S., & Mathew, B. 2022, MNRAS, 517, 3236, doi: [10.1093/mnras/stac2619](https://doi.org/10.1093/mnras/stac2619)
- Rajput, B., Shah, Z., Stalin, C. S., Sahayanathan, S., & Rakshit, S. 2021, MNRAS, 504, 1772, doi: [10.1093/mnras/stab970](https://doi.org/10.1093/mnras/stab970)
- Rajput, B., Stalin, C. S., & Sahayanathan, S. 2020, MNRAS, 498, 5128, doi: [10.1093/mnras/staa2708](https://doi.org/10.1093/mnras/staa2708)
- Rakshit, S. 2020, A&A, 642, A59, doi: [10.1051/0004-6361/202038324](https://doi.org/10.1051/0004-6361/202038324)
- Rakshit, S., Stalin, C. S., Muneer, S., Neha, S., & Paliya, V. S. 2017, ApJ, 835, 275, doi: [10.3847/1538-4357/835/2/275](https://doi.org/10.3847/1538-4357/835/2/275)
- Ramakrishnan, V., Hovatta, T., Tornikoski, M., et al. 2016, MNRAS, 456, 171, doi: [10.1093/mnras/stv2653](https://doi.org/10.1093/mnras/stv2653)
- Rees, M. J. 1984, ARA&A, 22, 471, doi: [10.1146/annurev.aa.22.090184.002351](https://doi.org/10.1146/annurev.aa.22.090184.002351)

- Ren, H. X., Cerruti, M., & Sahakyan, N. 2023, *Astronomy & Astrophysics*, 672, A86, doi: [10.1051/0004-6361/202244940](https://doi.org/10.1051/0004-6361/202244940)
- Rieger, F. M., & Volpe, F. 2010, *A&A*, 520, A23, doi: [10.1051/0004-6361/201014273](https://doi.org/10.1051/0004-6361/201014273)
- Romero, G. E., Cellone, S. A., & Combi, J. A. 1999, *A&AS*, 135, 477, doi: [10.1051/aas:1999184](https://doi.org/10.1051/aas:1999184)
- Romero, G. E., Cellone, S. A., Combi, J. A., & Andruchow, I. 2002, *A&A*, 390, 431, doi: [10.1051/0004-6361:20020743](https://doi.org/10.1051/0004-6361:20020743)
- Roy, A., Sarkar, A., Chatterjee, A., et al. 2022, *MNRAS*, 510, 3641, doi: [10.1093/mnras/stab3701](https://doi.org/10.1093/mnras/stab3701)
- Sahakyan, N. 2020, *Monthly Notices of the Royal Astronomical Society*, 496, 5518
- Saito, S., Stawarz, L., Tanaka, Y. T., et al. 2013, *ApJL*, 766, L11, doi: [10.1088/2041-8205/766/1/L11](https://doi.org/10.1088/2041-8205/766/1/L11)
- Sandrinelli, A., Covino, S., & Treves, A. 2014, *ApJL*, 793, L1, doi: [10.1088/2041-8205/793/1/L1](https://doi.org/10.1088/2041-8205/793/1/L1)
- Schneider, P., & Weiss, A. 1987, *A&A*, 171, 49
- Sillanpaa, A., Haarala, S., Valtonen, M. J., Sundelius, B., & Byrd, G. G. 1988, *ApJ*, 325, 628, doi: [10.1086/166033](https://doi.org/10.1086/166033)
- Smith, K. L., Mushotzky, R. F., Boyd, P. T., et al. 2018, *ApJ*, 857, 141, doi: [10.3847/1538-4357/aab88d](https://doi.org/10.3847/1538-4357/aab88d)
- Stalin, C. S., Kawabata, K. S., Uemura, M., et al. 2009, *MNRAS*, 399, 1357, doi: [10.1111/j.1365-2966.2009.15354.x](https://doi.org/10.1111/j.1365-2966.2009.15354.x)
- Sukanya, N., Stalin, C. S., Joseph, P., et al. 2018, *Journal of Astrophysics and Astronomy*, 39, 65, doi: [10.1007/s12036-018-9556-z](https://doi.org/10.1007/s12036-018-9556-z)
- Tandon, S. N., Ghosh, S. K., Hutchings, J., Stalin, C. S., & Subramaniam, A. 2017, *Current Science*, 113, 583, doi: [10.18520/cs/v113/i04/583-586](https://doi.org/10.18520/cs/v113/i04/583-586)
- Tandon, S. N., Postma, J., Joseph, P., et al. 2020, *AJ*, 159, 158, doi: [10.3847/1538-3881/ab72a3](https://doi.org/10.3847/1538-3881/ab72a3)
- Thompson, D. J., Djorgovski, S., & de Carvalho, R. 1990, *PASP*, 102, 1235, doi: [10.1086/132758](https://doi.org/10.1086/132758)
- Uchiyama, Y., Urry, C. M., Cheung, C. C., et al. 2006, *ApJ*, 648, 910, doi: [10.1086/505964](https://doi.org/10.1086/505964)
- Ulrich, M.-H., Maraschi, L., & Urry, C. M. 1997, *ARA&A*, 35, 445, doi: [10.1146/annurev.astro.35.1.445](https://doi.org/10.1146/annurev.astro.35.1.445)
- Urry, C. M., & Mushotzky, R. F. 1982, *ApJ*, 253, 38, doi: [10.1086/159607](https://doi.org/10.1086/159607)
- Urry, C. M., & Padovani, P. 1995, *PASP*, 107, 803, doi: [10.1086/133630](https://doi.org/10.1086/133630)
- Urry, C. M., Maraschi, L., Edelson, R., et al. 1993, *ApJ*, 411, 614, doi: [10.1086/172864](https://doi.org/10.1086/172864)
- Vagnetti, F., Trevese, D., & Nesci, R. 2003, *The Astrophysical Journal*, 590, 123
- Vagnetti, F., Trevese, D., & Nesci, R. 2003, *ApJ*, 590, 123, doi: [10.1086/374889](https://doi.org/10.1086/374889)
- Veron-Cetty, M.-P., & Veron, P. 2010, *Astronomy and Astrophysics*, 518, A10, doi: [10.1051/0004-6361/201014188](https://doi.org/10.1051/0004-6361/201014188)
- Villata, M., Raiteri, C. M., Kurtanidze, O. M., et al. 2002, *A&A*, 390, 407, doi: [10.1051/0004-6361:20020662](https://doi.org/10.1051/0004-6361:20020662)
- . 2004, *A&A*, 421, 103, doi: [10.1051/0004-6361:20035895](https://doi.org/10.1051/0004-6361:20035895)
- Wagner, S. J., & Witzel, A. 1995, *ARA&A*, 33, 163, doi: [10.1146/annurev.aa.33.090195.001115](https://doi.org/10.1146/annurev.aa.33.090195.001115)
- Webb, J. R. 2021, *Galaxies*, 9, 69
- Welsh, B. Y., Wheatley, J. M., & Neil, J. D. 2011, *A&A*, 527, A15, doi: [10.1051/0004-6361/201015865](https://doi.org/10.1051/0004-6361/201015865)
- Yuan, Q., Kushwaha, P., Gupta, A. C., et al. 2023, *ApJ*, 953, 47, doi: [10.3847/1538-4357/acdd74](https://doi.org/10.3847/1538-4357/acdd74)
- Zeng, W., Hu, W., Zhang, G.-M., et al. 2019, *PASP*, 131, 074102, doi: [10.1088/1538-3873/ab200f](https://doi.org/10.1088/1538-3873/ab200f)
- Zhang, Z., Gupta, A. C., Gaur, H., et al. 2021, *ApJ*, 909, 103, doi: [10.3847/1538-4357/abdd38](https://doi.org/10.3847/1538-4357/abdd38)

APPENDIX

A. BRIGHTNESS MEASUREMENTS OF THE SOURCE PKS 0208–512

Date	Filter	UTstart	UTend	Mag
30-10-2016	F148W	57690.991247	57690.998305	18.28 ± 0.05
		57691.063816	57691.067698	18.37 ± 0.07
		57691.249972	57691.253182	18.42 ± 0.08
		57691.385321	57691.386868	18.50 ± 0.12
		57691.588337	57691.600612	18.22 ± 0.05
	F169M	57691.723686	57691.731484	18.25 ± 0.07
		57690.991175	57690.998355	17.31 ± 0.07
		57691.063744	57691.067748	17.39 ± 0.09
		57691.249923	57691.253181	17.38 ± 0.10
		57691.317597	57691.324360	17.44 ± 0.07
25-12-2019	N219M	57691.385272	57691.386868	17.33 ± 0.14
		57691.520614	57691.524076	17.53 ± 0.10
		57691.588288	57691.600612	17.09 ± 0.05
		57691.655962	57691.657762	16.93 ± 0.12
		57691.723637	57691.731484	17.09 ± 0.06
	F172M	57691.791305	57691.793444	17.06 ± 0.12
		57691.862352	57691.863146	17.04 ± 0.19
		58841.831743	58841.833213	18.61 ± 0.13
		58841.904312	58841.905736	18.55 ± 0.15
		58841.976881	58841.985370	18.11 ± 0.06
		58842.305330	58842.311886	18.17 ± 0.07
		58842.643654	58842.654596	17.91 ± 0.09

B. BRIGHTNESS MEASUREMENTS OF THE
SOURCE 1ES 0229+200

C. BRIGHTNESS MEASUREMENTS OF THE
SOURCE OJ 287

Date	Filter	UTstart	UTend	Mag	Date	Filter	UTstart	UTend	Mag
01-10-2017	F154W	58027.768812	58027.790965	20.43 ± 0.10	10-04-2017	F169M	57852.921707	57852.931896	16.50 ± 0.03
		58027.838336	58027.850038	20.35 ± 0.10			57852.996559	57853.001230	16.42 ± 0.04
		58027.910905	58027.926301	20.44 ± 0.12			57853.124063	57853.127295	16.54 ± 0.05
		58027.768763	58027.791014	19.77 ± 0.05			57853.193861	57853.200357	16.52 ± 0.03
		58027.838287	58027.858677	19.84 ± 0.06			57853.263652	57853.273780	16.48 ± 0.03
		58027.910856	58027.926351	19.89 ± 0.07			57853.333450	57853.347202	16.48 ± 0.02
	N245M	58096.737591	58096.743303	20.23 ± 0.17			57853.407498	57853.420388	16.43 ± 0.02
		58096.789544	58096.810980	20.27 ± 0.09			57853.473045	57853.483899	16.47 ± 0.03
		58096.859519	58096.878642	20.46 ± 0.11			57853.542843	57853.551586	16.49 ± 0.03
		58096.932088	58096.944207	20.62 ± 0.15			57853.612640	57853.629733	16.51 ± 0.02
		58096.737542	58096.743352	20.00 ± 0.11			57853.682439	57853.686358	16.40 ± 0.04
09-12-2017	F154W	58096.789495	58096.811030	19.89 ± 0.06	N245M	N245M	57852.921656	57852.931948	15.84 ± 0.01
		58096.859470	58096.878692	19.91 ± 0.06			57852.997824	57853.001281	15.84 ± 0.02
		58096.932039	58096.944257	19.95 ± 0.08			57853.124012	57853.127347	15.80 ± 0.02
		58108.834869	58108.853240	20.44 ± 0.11			57853.193810	57853.200408	15.83 ± 0.01
		58108.907438	58108.920891	20.35 ± 0.12			57853.263602	57853.273830	15.80 ± 0.01
	N245M	58109.104261	58109.109884	20.42 ± 0.19			57853.333399	57853.347253	15.81 ± 0.01
		58109.171930	58109.180995	20.42 ± 0.15			57853.409942	57853.415465	15.79 ± 0.02
		58108.834820	58108.853290	19.89 ± 0.06			57853.417144	57853.420440	15.71 ± 0.02
		58108.907389	58108.920941	19.99 ± 0.07			57853.472995	57853.483899	15.70 ± 0.02
		58108.979959	58108.988579	19.89 ± 0.09			57853.542792	57853.551586	15.71 ± 0.02
22-12-2017	F154W	58109.052528	58109.056241	19.99 ± 0.14			57853.612590	57853.629784	15.73 ± 0.01
		58109.104212	58109.109934	19.91 ± 0.11			57853.682388	57853.686437	15.71 ± 0.02
		58109.171881	58109.181045	20.03 ± 0.09			57853.729287	57894.732999	16.05 ± 0.03
		58126.562901	58126.577813	20.36 ± 0.12			57894.729287	57894.732999	16.05 ± 0.03
		58126.630575	58126.645463	20.34 ± 0.11			57894.734732	57894.740242	15.95 ± 0.02
	N245M	58126.698249	58126.713114	20.40 ± 0.12			57894.796957	57894.807898	16.01 ± 0.02
		58126.765924	58126.779650	20.13 ± 0.11			57894.868199	57894.875548	15.96 ± 0.02
		58126.562852	58126.577862	19.86 ± 0.07			57894.940768	57894.943199	15.96 ± 0.04
		58126.630526	58126.645513	19.78 ± 0.06			57895.202923	57895.213006	15.98 ± 0.02
		58126.698201	58126.713163	19.87 ± 0.07			57895.270585	57895.281451	15.98 ± 0.02
08-01-2018	F154W	58126.765875	58126.779700	19.70 ± 0.06			57895.338248	57895.349101	15.99 ± 0.02
		58984.390970	58984.396566	16.03 ± 0.02			57895.405932	57895.407435	15.85 ± 0.04
		58984.458633	58984.469640	16.10 ± 0.02			57895.471746	57895.481214	16.11 ± 0.02
		58984.526301	58984.537291	16.09 ± 0.02			57895.537291	57895.548151	16.08 ± 0.02
		58984.593963	58984.604941	16.06 ± 0.02			57895.604941	57895.615861	16.07 ± 0.03
	F148W	58984.661625	58984.664079	16.07 ± 0.03			57895.664079	57895.675548	16.08 ± 0.02
		58984.729287	57894.732999	16.05 ± 0.03			57895.729287	57895.740242	15.95 ± 0.02
		58984.734732	57894.740242	15.95 ± 0.02			57895.796957	57895.807898	16.01 ± 0.02
		58984.807898	57894.8199	15.96 ± 0.02			57895.868199	57895.881999	15.97 ± 0.02
		57894.875548	57894.881999	15.96 ± 0.02			57895.940768	57895.943199	15.96 ± 0.04
18-05-2020	F148W	57894.940768	57894.943199	15.96 ± 0.04		F172M	57896.827577	57896.837416	15.70 ± 0.04
		57895.202923	57895.213006	15.98 ± 0.02			57896.900145	57896.905066	15.68 ± 0.05
		57895.270585	57895.281451	15.98 ± 0.02			57897.165157	57897.172383	15.62 ± 0.04
		57895.338248	57895.349101	15.99 ± 0.02			57897.232825	57897.243306	15.58 ± 0.03
		57895.405932	57895.407435	15.85 ± 0.04			57897.300488	57897.310956	15.54 ± 0.03
	F172M	57896.827577	57896.837416	15.70 ± 0.04			57897.368156	57897.378613	15.61 ± 0.04
		57896.900145	57896.905066	15.68 ± 0.05			57897.435818	57897.446263	15.60 ± 0.04
		57897.165157	57897.172383	15.62 ± 0.04			57897.503480	57897.505199	15.69 ± 0.08
		57897.232825	57897.243306	15.58 ± 0.03			57897.638812	57897.649214	15.55 ± 0.03
		57897.300488	57897.310956	15.54 ± 0.03			57897.706479	57897.710244	15.59 ± 0.05
F148Wa	F148Wa	57897.368156	57897.378613	15.61 ± 0.04		F148Wa	57898.409168	57898.416746	16.12 ± 0.02
		57897.435818	57897.446263	15.60 ± 0.04			57898.473572	57898.481214	16.11 ± 0.02
		57897.503480	57897.505199	15.69 ± 0.08			57898.5608902	57898.5619709	16.10 ± 0.02
		57897.638812	57897.649214	15.55 ± 0.03			57898.5676565	57898.5687359	16.10 ± 0.02
		57897.706479	57897.710244	15.59 ± 0.05			57898.5744227	57898.5748966	16.10 ± 0.02
		57898.5556185	57898.561064	16.03 ± 0.02			57898.5896556185	57898.5986561064	16.03 ± 0.02

Date	Filter	UTstart	UTend	Mag
18-04-2018	F169M	58225.694593	58225.707433	17.14 ± 0.03
		58225.758997	58225.775095	17.12 ± 0.03
		58225.827579	58225.842745	17.17 ± 0.03
		58225.900148	58225.910402	17.12 ± 0.04
		58225.972717	58225.977893	17.15 ± 0.05
		58226.232633	58226.240782	17.15 ± 0.04
		58226.300301	58226.316327	17.07 ± 0.03
		58226.367963	58226.383990	17.11 ± 0.03
		58226.435625	58226.451641	17.10 ± 0.03
		58226.503294	58226.519303	17.10 ± 0.03
		58226.570956	58226.586954	17.06 ± 0.03
		58226.638618	58226.654616	17.03 ± 0.03
		58226.706281	58226.722266	17.08 ± 0.03
		58226.773949	58226.789928	17.09 ± 0.03
		58226.843550	58226.857579	17.18 ± 0.03
		58226.916119	58226.925241	17.22 ± 0.04
		58226.988688	58226.992891	17.18 ± 0.06
		58227.179928	58227.183148	17.21 ± 0.07
		58227.247590	58227.259189	17.19 ± 0.04
		58227.315253	58227.331167	17.11 ± 0.03
		58227.382921	58227.398818	17.15 ± 0.03
		58227.450583	58227.466479	17.19 ± 0.03
		58227.518251	58227.534130	17.12 ± 0.03
		58227.585913	58227.596754	17.16 ± 0.04
F172M		58223.458444	58223.461745	16.81 ± 0.09
		58223.526112	58223.542435	16.92 ± 0.05
		58223.593774	58223.610092	16.89 ± 0.05
		58223.661437	58223.677748	16.88 ± 0.05
		58223.729099	58223.745405	16.96 ± 0.05
		58223.796775	58223.813061	16.94 ± 0.05
		58223.867850	58223.880717	16.98 ± 0.05
		58223.940425	58223.948374	16.94 ± 0.07
		58224.202735	58224.206411	16.94 ± 0.09
		58224.270403	58224.281060	17.10 ± 0.06
		58224.338065	58224.354312	17.01 ± 0.05
		58224.405728	58224.421968	16.92 ± 0.05
		58224.473390	58224.489624	17.00 ± 0.05
		58224.541052	58224.557281	16.98 ± 0.05
		58224.608720	58224.624937	17.04 ± 0.05
		58224.676383	58224.692593	16.94 ± 0.05
		58224.811721	58224.827906	16.97 ± 0.05
		58224.884171	58224.895546	16.99 ± 0.06
		58224.956740	58224.963219	17.06 ± 0.08
		58225.217688	58225.223425	16.92 ± 0.07
		58225.285349	58225.299468	16.94 ± 0.05
		58225.353011	58225.369157	16.95 ± 0.05
		58225.420680	58225.436807	17.03 ± 0.05
		58225.488342	58225.504464	16.99 ± 0.05
		58225.556004	58225.572126	16.98 ± 0.05
		58225.623666	58225.632778	16.90 ± 0.06
		58225.691329	58225.692828	17.02 ± 0.15

D. BRIGHTNESS MEASUREMENTS OF THE SOURCE 1ES 1101–232

Date	Filter	UTstart	UTend	Mag
30-12-2016	F154W	57750.400520	57750.416409	18.39 ± 0.04
		57750.468182	57750.484078	18.44 ± 0.04
		57750.535845	57750.551746	18.39 ± 0.04
		57750.603507	57750.619414	18.42 ± 0.04
		57750.671163	57750.687082	18.42 ± 0.04
		57750.738825	57750.754751	18.46 ± 0.04
		57750.806482	57750.822419	18.52 ± 0.05
		57750.874144	57750.890087	18.46 ± 0.04
		57750.944243	57750.957755	18.44 ± 0.05
		57751.016812	57751.025423	18.51 ± 0.06
		57751.089381	57751.093092	18.41 ± 0.09
		57751.144787	57751.147032	18.71 ± 0.13
		57751.212450	57751.219254	18.51 ± 0.07
		57751.280106	57751.291130	18.43 ± 0.05
		57751.347768	57751.362313	18.44 ± 0.05
		57751.415431	57751.428900	18.43 ± 0.04
		57751.483093	57751.499101	18.49 ± 0.05
		57751.550749	57751.566769	18.44 ± 0.04
		57751.618411	57751.634437	18.39 ± 0.04
		57751.686074	57751.702111	18.40 ± 0.04
		57751.753730	57751.769779	18.34 ± 0.04
		57751.821392	57751.837447	18.47 ± 0.04
		57751.889056	57751.905110	18.40 ± 0.04
		57751.960558	57751.972778	18.43 ± 0.05
		57752.033133	57752.040446	18.44 ± 0.06
		57752.105702	57752.108114	18.38 ± 0.11
		57752.159686	57752.163003	18.29 ± 0.09
		57752.229222	57752.235231	18.40 ± 0.07
		57752.295010	57752.306408	18.45 ± 0.05
		57752.362673	57752.377590	18.43 ± 0.05
N263M		57752.430329	57752.446455	18.40 ± 0.04
		57752.497991	57752.501664	18.55 ± 0.10
		57750.400471	57750.416460	17.93 ± 0.03
		57750.468133	57750.484127	17.89 ± 0.03
		57750.535796	57750.551795	17.88 ± 0.03
		57750.603458	57750.619464	17.84 ± 0.03
		57750.671114	57750.687132	17.91 ± 0.03
		57750.738777	57750.754800	17.92 ± 0.03
		57750.806433	57750.822468	17.90 ± 0.03
		57750.874095	57750.890136	17.90 ± 0.03
		57750.944195	57750.957805	17.91 ± 0.03
		57751.016764	57751.025473	17.91 ± 0.04
		57751.089333	57751.093141	17.89 ± 0.06
		57751.144739	57751.147082	17.92 ± 0.07
		57751.212401	57751.219304	17.92 ± 0.04
		57751.280057	57751.291180	17.85 ± 0.03
		57751.347719	57751.362362	17.90 ± 0.03
		57751.415382	57751.431482	17.92 ± 0.03
		57751.483044	57751.499150	17.94 ± 0.03
		57751.550700	57751.566818	17.93 ± 0.03
		57751.618363	57751.634487	17.91 ± 0.03
		57751.686025	57751.702161	17.93 ± 0.03
		57751.753681	57751.769829	17.96 ± 0.03
		57751.821343	57751.837497	17.93 ± 0.03

Date	Filter	UTstart	UTend	Mag
		57751.889007	57751.905159	17.93 ± 0.03
		57751.960509	57751.972827	17.95 ± 0.03
		57752.033084	57752.040496	17.98 ± 0.04
		57752.105653	57752.108164	17.82 ± 0.07
		57752.159637	57752.163053	18.05 ± 0.07
		57752.227299	57752.235281	17.95 ± 0.04
		57752.294961	57752.306457	17.86 ± 0.03
		57752.362624	57752.377640	17.96 ± 0.03
		57752.430280	57752.446505	17.90 ± 0.03
		57752.497942	57752.501714	18.04 ± 0.06

E. BRIGHTNESS MEASUREMENTS OF THE SOURCE 1ES 1218+304

Date	Filter	UTstart	UTend	Mag
21-05-2016	F148W	57528.302435	57528.308327	17.88 ± 0.05
		57528.372248	57528.383183	17.91 ± 0.04
		57528.442067	57528.458041	17.99 ± 0.03
		57528.511879	57528.529370	17.93 ± 0.03
		57528.581692	57528.599164	17.88 ± 0.03
		57528.651504	57528.668952	17.90 ± 0.03
		57528.721317	57528.738740	17.92 ± 0.03
		57528.791136	57528.808534	17.90 ± 0.03
		57528.861914	57528.878322	17.96 ± 0.03
		57528.936769	57528.948117	17.94 ± 0.04
		57529.011625	57529.017904	17.91 ± 0.05
		57529.279823	57529.281816	17.82 ± 0.08
		57529.419509	57529.431526	17.90 ± 0.03
N245M		57528.302745	57528.308378	17.41 ± 0.03
		57528.373033	57528.383234	17.36 ± 0.02
		57528.442016	57528.458092	17.38 ± 0.02
		57528.511829	57528.529421	17.36 ± 0.02
		57528.581641	57528.599215	17.39 ± 0.02
		57528.651454	57528.669003	17.36 ± 0.02
		57528.721266	57528.738792	17.38 ± 0.02
		57528.791085	57528.808586	17.38 ± 0.02
		57528.861863	57528.878374	17.38 ± 0.02
		57528.936719	57528.948168	17.39 ± 0.02
		57529.011574	57529.017956	17.36 ± 0.03
		57529.279773	57529.281867	17.42 ± 0.05
		57529.419913	57529.431577	17.35 ± 0.02

F. BRIGHTNESS MEASUREMENTS OF THE SOURCE H 1426+428

Date	Filter	UTstart	UTend	Mag
05-03-2018	F148W	58181.865544	58181.867427	18.47 ± 0.11
		58181.919243	58181.935090	18.65 ± 0.04
		58181.991811	58181.998758	18.60 ± 0.06
		58182.064381	58182.070426	18.53 ± 0.06
		58182.253915	58182.261613	18.63 ± 0.06
		58182.321565	58182.337656	18.64 ± 0.04
		58182.389210	58182.408744	18.63 ± 0.04
		58182.456859	58182.463086	18.66 ± 0.07
F154W		58181.577434	58181.596767	18.58 ± 0.04
		58181.645079	58181.664441	18.50 ± 0.04
		58181.712729	58181.732103	18.56 ± 0.04
		58181.780374	58181.799771	18.47 ± 0.04
		58181.848025	58181.863807	18.52 ± 0.05
N242W		58181.577385	58181.596816	18.13 ± 0.01
		58181.645030	58181.664490	18.14 ± 0.01
		58181.712680	58181.732152	18.18 ± 0.01
		58181.780325	58181.781955	18.21 ± 0.05
		58181.783577	58181.799821	18.18 ± 0.03
N245M		58181.847977	58181.867477	18.19 ± 0.03
		58181.919194	58181.935139	18.23 ± 0.03
		58181.991762	58181.998808	18.16 ± 0.04
		58182.064332	58182.070476	18.19 ± 0.04
		58182.253866	58182.261659	18.16 ± 0.04
		58182.321516	58182.337706	18.20 ± 0.03
		58182.389161	58182.408793	18.15 ± 0.02
		58182.456810	58182.463086	18.25 ± 0.05

G. BRIGHTNESS MEASUREMENTS OF THE
SOURCE PKS 1510–089

Date	Filter	UTstart	UTend	Mag	Date	Filter	UTstart	UTend	Mag
30-03-2016	F172M	57476.398455	57476.400733	17.30 ± 0.14	15-06-2018	F172M	58192.878220	58192.896677	17.55 ± 0.05
		57476.455977	57476.473306	17.12 ± 0.05			58192.950788	58192.964340	17.55 ± 0.06
		57476.523622	57476.542681	17.09 ± 0.05			58193.023364	58193.032002	17.43 ± 0.06
		57476.591272	57476.610338	17.06 ± 0.05			58193.095933	58193.099664	17.93 ± 0.12
		57476.658923	57476.678000	17.09 ± 0.05			58193.215718	58193.225905	17.53 ± 0.06
		57476.726567	57476.745657	17.06 ± 0.05			58193.351025	58193.369307	17.53 ± 0.05
		57476.794218	57476.813313	17.05 ± 0.05			58193.418680	58193.437988	17.48 ± 0.05
		57476.864493	57476.880975	17.13 ± 0.05			58193.486332	58193.505650	17.58 ± 0.05
		57476.937062	57476.948632	17.08 ± 0.06			58193.553989	58193.573325	17.64 ± 0.05
		57477.082206	57477.083941	17.02 ± 0.14			58193.621639	58193.640987	17.55 ± 0.05
		57477.335410	57477.344146	17.16 ± 0.07			58193.689295	58193.696009	17.63 ± 0.08
		57477.403060	57477.416716	17.16 ± 0.06			15-06-2018	58284.086589	58284.089744
		57477.470711	57477.489285	17.08 ± 0.05			58284.154258	58284.159266	17.42 ± 0.10
		57477.538361	57477.557557	17.06 ± 0.05			58284.297771	58284.306408	17.33 ± 0.07
		57477.606018	57477.625214	17.09 ± 0.05			58284.357274	58284.377591	17.29 ± 0.05
		57477.673656	57477.692876	17.11 ± 0.05			58284.424942	58284.445639	17.32 ± 0.05
		57477.741307	57477.760532	17.09 ± 0.05			58284.492611	58284.513314	17.34 ± 0.05
		57477.808957	57477.828195	17.10 ± 0.05			58284.560285	58284.580982	17.28 ± 0.05
		57477.880471	57477.895851	17.09 ± 0.05			58284.627955	58284.648656	17.28 ± 0.05
		57477.953040	57477.963508	17.15 ± 0.06			58284.695628	58284.716318	17.29 ± 0.05
		57478.025609	57478.031161	17.05 ± 0.08			58284.763296	58284.771371	17.26 ± 0.07
N219M	N219M	57476.398407	57476.400783	17.33 ± 0.11			15-06-2018	58284.763296	58284.771371
		57476.455928	57476.473356	17.27 ± 0.04			15-06-2018	58284.763296	58284.771371
		57476.523573	57476.542731	17.34 ± 0.04			15-06-2018	58284.763296	58284.771371
		57476.591223	57476.610388	17.26 ± 0.04			15-06-2018	58284.763296	58284.771371
		57476.658874	57476.678049	17.38 ± 0.05			15-06-2018	58284.763296	58284.771371
		57476.726518	57476.745706	17.28 ± 0.04			15-06-2018	58284.763296	58284.771371
		57476.794169	57476.813362	17.28 ± 0.04			15-06-2018	58284.763296	58284.771371
		57476.864444	57476.881025	17.30 ± 0.05			15-06-2018	58284.763296	58284.771371
		57476.937013	57476.948681	17.31 ± 0.05			15-06-2018	58284.763296	58284.771371
		57477.082157	57477.083991	17.42 ± 0.13			15-06-2018	58284.763296	58284.771371
		57477.335361	57477.344196	17.27 ± 0.06			15-06-2018	58284.763296	58284.771371
		57477.403011	57477.416765	17.37 ± 0.05			15-06-2018	58284.763296	58284.771371
		57477.470662	57477.489334	17.31 ± 0.04			15-06-2018	58284.763296	58284.771371
		57477.538312	57477.557607	17.36 ± 0.04			15-06-2018	58284.763296	58284.771371
		57477.605967	57477.625263	17.37 ± 0.04			15-06-2018	58284.763296	58284.771371
		57477.673607	57477.692926	17.38 ± 0.04			15-06-2018	58284.763296	58284.771371
		57477.741258	57477.760582	17.32 ± 0.04			15-06-2018	58284.763296	58284.771371
		57477.808908	57477.828244	17.34 ± 0.04			15-06-2018	58284.763296	58284.771371
		57477.880422	57477.895901	17.43 ± 0.05			15-06-2018	58284.763296	58284.771371
		57477.952992	57477.963557	17.32 ± 0.06			15-06-2018	58284.763296	58284.771371
		57478.025561	57478.031211	17.42 ± 0.08			15-06-2018	58284.763296	58284.771371
16-03-2018	F172M	58192.878269	58192.896628	17.30 ± 0.05			15-06-2018	58284.763296	58284.771371
		58192.950836	58192.964290	17.30 ± 0.06			15-06-2018	58284.763296	58284.771371
		58193.023413	58193.031953	17.24 ± 0.07			15-06-2018	58284.763296	58284.771371
		58193.095982	58193.099615	17.14 ± 0.10			15-06-2018	58284.763296	58284.771371
		58193.215767	58193.225855	17.30 ± 0.07			15-06-2018	58284.763296	58284.771371
		58193.351074	58193.369257	17.17 ± 0.05			15-06-2018	58284.763296	58284.771371
		58193.418729	58193.437939	17.26 ± 0.05			15-06-2018	58284.763296	58284.771371
		58193.486381	58193.505601	17.30 ± 0.05			15-06-2018	58284.763296	58284.771371
		58193.554037	58193.573275	17.26 ± 0.05			15-06-2018	58284.763296	58284.771371
		58193.621688	58193.640937	17.35 ± 0.05			15-06-2018	58284.763296	58284.771371
		58193.689344	58193.695960	17.36 ± 0.08			15-06-2018	58284.763296	58284.771371

H. BRIGHTNESS MEASUREMENTS OF THE
SOURCE Mrk 501

Date	Filter	UTstart	UTend	Mag
15-08-2016	F154W	57615.260263	57615.269143	15.82 ± 0.02
		57615.323334	57615.337866	15.83 ± 0.02
		57615.391014	57615.405528	15.84 ± 0.02
		57615.458688	57615.473184	15.85 ± 0.02
		57615.526368	57615.540841	15.84 ± 0.02
		57615.594042	57615.608497	15.84 ± 0.02
		57615.661723	57615.676160	15.86 ± 0.02
		57615.729396	57615.743816	15.85 ± 0.02
		57615.797070	57615.811472	15.84 ± 0.02
		57615.867618	57615.879134	15.87 ± 0.02
		57615.940187	57615.946790	15.84 ± 0.02
N219M		57615.255611	57615.269193	15.54 ± 0.03
		57615.323285	57615.337916	15.57 ± 0.03
		57615.390965	57615.405578	15.54 ± 0.03
		57615.458639	57615.473234	15.54 ± 0.03
		57615.526319	57615.540891	15.58 ± 0.03
		57615.593993	57615.608547	15.56 ± 0.03
		57615.661675	57615.676209	15.53 ± 0.03
		57615.729347	57615.743866	15.53 ± 0.03
		57615.797021	57615.811522	15.59 ± 0.03
		57615.867569	57615.879184	15.57 ± 0.03
		57615.940138	57615.946840	15.50 ± 0.03
28-03-2020	F148W	58935.275928	58935.281755	16.09 ± 0.02
		58935.343573	58935.355761	16.05 ± 0.02
		58935.817072	58935.833668	16.08 ± 0.02
		58935.884736	58935.889611	16.08 ± 0.02
		58936.028618	58936.036643	16.11 ± 0.02
		58936.101187	58936.104294	16.07 ± 0.03
		58936.290578	58936.297587	16.06 ± 0.02
		58936.493506	58936.510244	16.11 ± 0.02
		58936.561150	58936.577906	16.09 ± 0.02
		58936.628789	58936.645556	16.10 ± 0.02
		58936.696433	58936.713219	16.09 ± 0.02
		58936.764078	58936.780881	16.10 ± 0.02
		58936.831716	58936.848530	16.08 ± 0.02
		58936.899451	58936.916194	16.08 ± 0.02
		58936.972020	58936.983856	16.08 ± 0.02
		58937.044589	58937.051507	16.11 ± 0.02
		58937.117158	58937.119169	16.10 ± 0.04
		58937.237571	58937.241479	16.05 ± 0.03
		58937.305216	58937.317871	16.11 ± 0.02
		58937.372861	58937.389794	16.11 ± 0.02
		58937.440499	58937.457457	16.08 ± 0.02
		58937.508144	58937.525106	16.09 ± 0.02
		58937.575788	58937.592769	16.10 ± 0.02
		58937.643427	58937.660426	16.09 ± 0.02
		58937.711065	58937.726873	16.10 ± 0.02

I. BRIGHTNESS MEASUREMENTS OF THE
SOURCE PKS 2155–304

Date	Filter	UTstart	UTend	Mag
21-05-2018	F154W	58259.329918	58259.332444	15.25 ± 0.03
		58259.397568	58259.405364	15.31 ± 0.02
		58259.465217	58259.478016	15.29 ± 0.01
		58259.532863	58259.544023	15.29 ± 0.02
24-06-2018	F154W	58293.495067	58293.513388	15.17 ± 0.01
		58293.562712	58293.579373	15.17 ± 0.01
16-09-2019	F154W	58742.573283	58742.593529	15.02 ± 0.01
		58742.639023	58742.643320	15.04 ± 0.02
		58742.774366	58742.777812	14.99 ± 0.02

J. BRIGHTNESS MEASUREMENTS OF THE
SOURCE 1ES 2344+514

Date	Filter	UTstart	UTend	Mag
06-06-2017	F172M	57910.717527	57910.727655	18.71 ± 0.13
		57910.787165	57910.797305	18.44 ± 0.11
		57910.856803	57910.863068	20.05 ± 0.34
	N245M	57910.717477	57910.727707	18.23 ± 0.04
		57910.787115	57910.797356	18.18 ± 0.04
		57910.856752	57910.860639	18.19 ± 0.06
09-07-2017	F172M	57943.391924	57943.405146	18.36 ± 0.10
		57943.464512	57943.479844	18.54 ± 0.10
		57943.531900	57943.546931	18.58 ± 0.10
	N245M	57943.391873	57943.405197	18.25 ± 0.03
		57943.465318	57943.479895	18.18 ± 0.03
		57943.531849	57943.549083	18.18 ± 0.03
07-08-2017	F172M	57972.282651	57972.300458	18.60 ± 0.10
		57972.352620	57972.374054	18.53 ± 0.08
		57972.422583	57972.430529	18.45 ± 0.13
	N245M	57972.282601	57972.300509	18.11 ± 0.03
		57972.352569	57972.374105	18.10 ± 0.02
		57972.422532	57972.428121	18.12 ± 0.05
07-09-2017	F172M	58003.815110	58003.837802	18.87 ± 0.10
		58003.889949	58003.907581	19.02 ± 0.12
		58003.964788	58003.972611	19.13 ± 0.19
	N245M	58003.815060	58003.837853	18.60 ± 0.03
		58003.889899	58003.907632	18.65 ± 0.03
		58003.964738	58003.972663	18.63 ± 0.05
22-11-2017	N245M	58078.933083	58078.942454	18.56 ± 0.04
		58079.005652	58079.010116	18.59 ± 0.06
		58079.127772	58079.130418	18.59 ± 0.08
		58079.195446	58079.201251	18.48 ± 0.05
07-12-2017	F172M	58094.972718	58094.978781	18.62 ± 0.16
		58095.233275	58095.243561	19.03 ± 0.15
	N245M	58094.972670	58094.978831	18.40 ± 0.05
		58095.233226	58095.243611	18.37 ± 0.04
12-09-2018	F172M	58372.864037	58372.882670	18.81 ± 0.10
		58372.936606	58372.950332	18.58 ± 0.11
		58373.009175	58373.017994	18.78 ± 0.15
		58373.063674	58373.064969	18.73 ± 0.37